Mixing and Spreading of the Mediterranean Outflow

MOLLY O'NEIL BARINGER

NOAA/Atlantic Oceanographic and Meteorological Laboratory, Miami, Florida

JAMES F. PRICE

Woods Hole Oceanographic Institution, Woods Hole, Massachusetts

(Manuscript received 3 March 1996, in final form 28 January 1997)

ABSTRACT

Hydrographic and current profiler data taken during the 1988 Gulf of Cadiz Expedition have been analyzed to diagnose the mixing, spreading, and descent of the Mediterranean outflow. The θ–S properties and the thickness and width of the outflow were similar to that seen in earlier surveys. The transport of pure Mediterranean Water (i.e., water with $S \geq 38.4$ psu) was estimated to be about 0.4×10^6 m^3 s^{-1}, which is lower than historical estimates—most of which were indirect—but comparable to other recent estimates made from direct velocity observations.

The outflow transport estimated at the west end of the Strait of Gibraltar was about 0.7×10^6 m^3 s^{-1} of mixed water, and the transport increased to about 1.9×10^6 m^3 s^{-1} within the eastern Gulf of Cadiz. This increase in transport occurred by entrainment of fresher North Atlantic Central Water, and the salinity anomaly of the outflow was consequently reduced. The velocity-weighted salinity decreased to 36.7 psu within 60 km of the strait and decreased by about another 0.1 before the deeper portion of the outflow began to separate from of the bottom near Cape St. Vincent. Entrainment appears to have been correlated spatially with the initial descent of the continental slope and with the occurrence of bulk Froude numbers slightly greater than 1. In the western Gulf of Cadiz, where entrainment was much weaker, Froude numbers were consistently well below 1.

The outflow began in the eastern Strait of Gibraltar as a narrow (10 km wide) current having a very narrow range of θ–S properties. The outflow broadened as it descended the continental slope of the northern Gulf of Cadiz and reached a maximum width of 80 km in the western Gulf of Cadiz. The descent of the outflow was very asymmetric: The southern (offshore) edge of the outflow descended about 1000 m from Gibraltar to Cape St. Vincent, while the northern (onshore) edge of the outflow descended only a few hundred meters. The northern, onshore side thus remained considerably higher in the water column and thus entrained relatively warm North Atlantic Central Water. This caused the outflow to develop horizontal θ–S variability and, by about 140 km downstream, the across-stream variation in temperature on an isopycnal was more than 2°C.

Much of the volume transport in the western Gulf of Cadiz was contained within two preferred modes or cores. The deeper, offshore core had a central $\sigma_\theta = 27.8$ kg m^{-3}, and the shallower onshore core, which was still in contact with the bottom in the Gulf of Cadiz, had a central $\sigma_\theta = 27.5$ kg m^{-3}. These two cores develop as a result of the spreading and horizontally varying entrainment noted above, combined with topographic steering.

1. A new look at the Mediterranean outflow

The source waters of the Mediterranean outflow are intermediate and deep waters of the western Mediterranean Sea that are highly saline, $S \geq 38.4$ psu, and consequently very dense, $\sigma_\theta \geq 28.95$ kg m^{-3}. As this Mediterranean Water flows westward through the Strait of Gibraltar and the Gulf of Cadiz, it mixes with and entrains the overlying North Atlantic Central Water. This entrainment causes the salinity and density of the Mediterranean outflow water to decrease substantially. The mixed Mediterranean Water that finally reaches Cape St. Vincent and the open North Atlantic has a salinity of about $36.35 \leq S \leq 36.65$ psu and a density of about $27.3 \leq \sigma_\theta \leq 27.7$ kg m^{-3}, which make it neutrally buoyant in the lower North Atlantic thermocline (Fig. 1) (Wust 1935; Worthington and Wright 1970; Reid 1979).

Our goal is to describe the geography and the dynamics of this important mixing process by analysis of field data taken during the 1988 Gulf of Cadiz expedition (Kennelly et al. 1989a). These data are closely spaced CTD, expendable current profiler (XCP), and expendable dissipation profiler (XDP) casts. These later data are the first of their kind within the Mediterranean outflow. The primary objective of the field program was

Corresponding author address: Dr. M. Baringer, NOAA/Atlantic Oceanographic and Meteorological Laboratory, 4301 Rickenbacker Causeway, Miami, FL 33149.
E-mail: baringer@aoml.noaa.gov

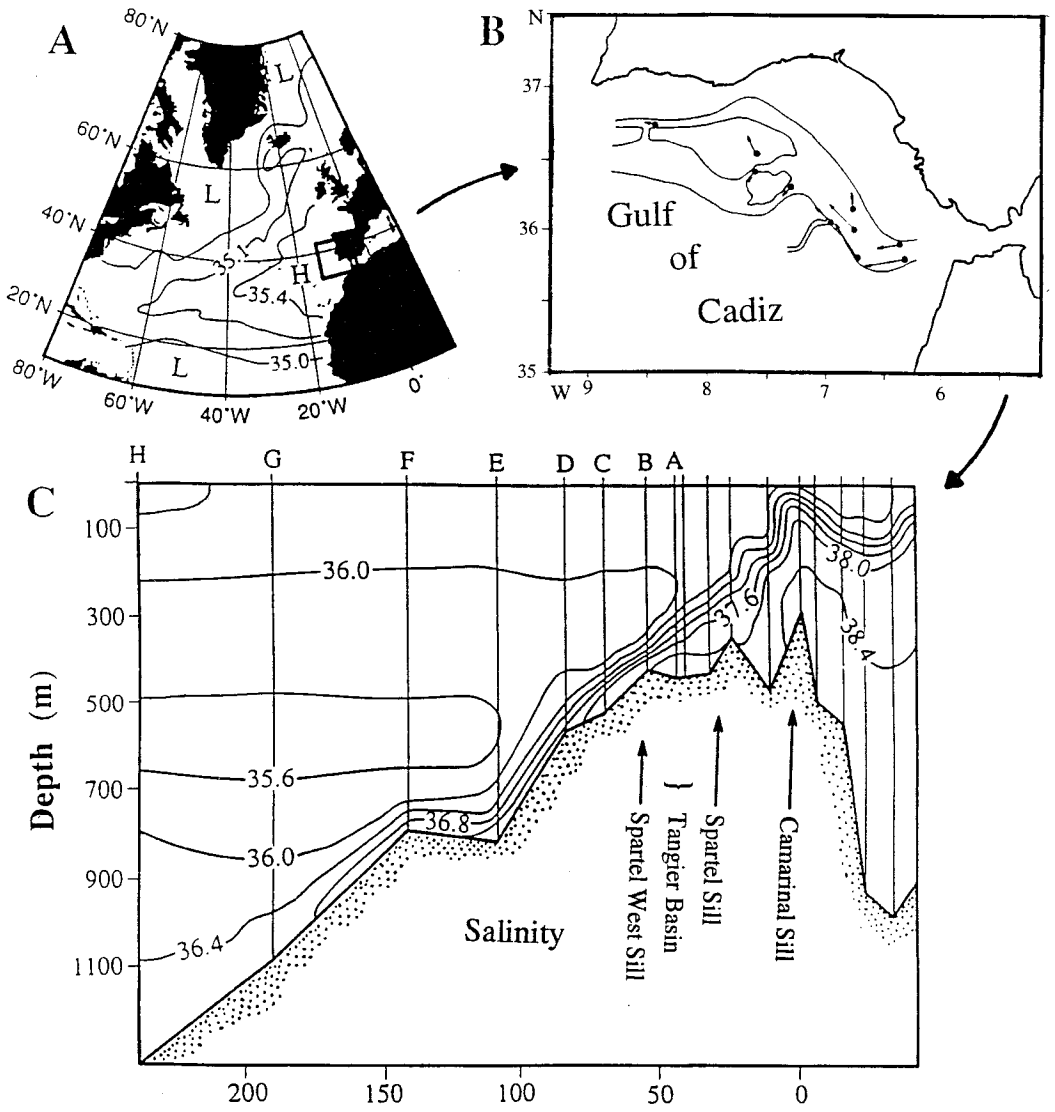

FIG. 1. Three views of the Mediterranean outflow: (a). Salinity on the 27.69 σ_θ density surface in the North Atlantic [adapted from Fig. 2 of Reid (1979)]. This surface is at a depth of about 1200 m on average in the subtropical North Atlantic and closely follows the subsurface salinity maximum characteristic of the Mediterranean water. (b) Schematic showing the salinity of the Mediterranean outflow in the Gulf of Cadiz reproduced from Madelain (1970). Current velocities (arrows) are short duration measurements taken during 1965–67 aboard the *Job Ha Zelian*, the *Calypso*, and the *Jean Charcot*. (c) Composite section along the axis of the Mediterranean outflow made from data presented here, following stations with the maximum salinity (some profiles are in Fig. 3). This section follows the lower, deeper core of the Mediterranean outflow (discussed in section 4c). The 36.4 isohaline approximately defines the top of the Mediterranean outflow in the Gulf of Cadiz. Within the strait, however, the top of the outflow is better demarked with the 37.0 isohaline whose depth varies considerably with the M_2 tide (Bryden et al. 1989). In this section the 37.0 isohaline surface is at a depth of 18 m at the Camarinal Sill, suggesting that this section is probably not representative of the time-averaged mean within the Strait of Gibraltar (as discussed more fully in section 2c).

to obtain sufficient observations to be able to tell where and why mixing occurred in the Mediterranean outflow. There was some emphasis on the eastern Gulf of Cadiz where we suspected that the mixing was most intense. Several studies of these data have already been presented and made use of here; Price et al. (1993) gave a brief description of this dataset and a preliminary discussion of the dynamics of the outflow. Johnson et al. (1994a, b) used the current and dissipation data to estimate bottom and interfacial stresses, which are crucial elements of the dynamics.

The plan for this paper is as follows; in section 2 we describe the sampling of the field experiment and take a first look at the observations. The horizontal spreading of the outflow is examined in section 3, and the downstream evolution of the property fluxes is examined in

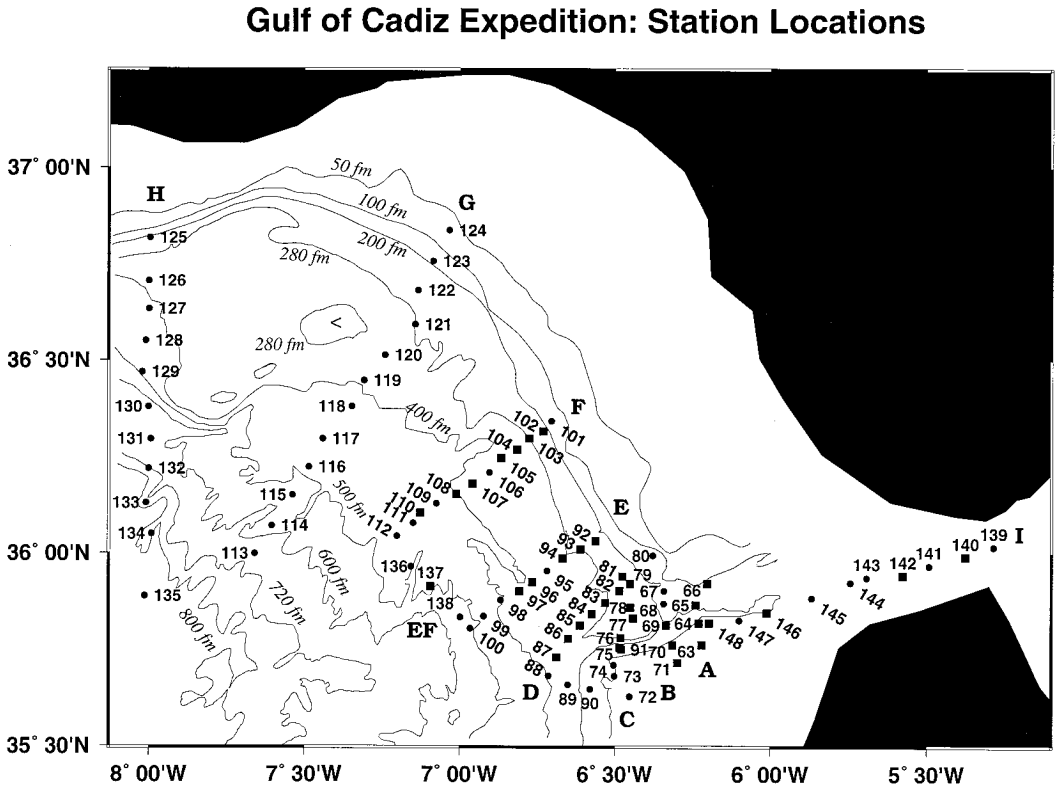

FIG. 2. Station plan of CTD and XCP locations. Stations marked with squares include XCP profiles. Gulf of Cadiz bathymetry adapted from Kenyon and Belderson (1973), with depth given in fathoms (1 fm = 1.83 m). See Fig. 1 to see the Gulf of Cadiz in a larger context.

section 4. The dominant modification of the outflow is found to occur by entrainment in a limited area close to the Strait of Gibraltar. One possible cause for this vigorous entrainment is that the current appears to be unstable to Kelvin–Helmholtz waves, which we examine in section 5. Section 6 concludes with a summary and remarks.

2. An overview of the observations

This paper examines the Mediterranean outflow in the central and eastern Gulf of Cadiz using 98 CTD casts (Fig. 2) obtained with a Sea-Bird electronics CTD and 47 in situ XCPs (Sanford et al. 1993; Kennelly et al. 1989a; Kennelly et al. 1989b; Kennelly et al. 1989c). Most of the CTD stations were laid out in eight sections, labeled A–H, that were approximately normal to the outflow and in one section, I, which was along the axis of the Strait of Gibraltar. Sections A–H were extended far enough that at least one station on each end of the sections showed no sign of the high salinity outflow water, thus sampling the entire outflow. These sections covered the first 250 km of the outflow's path in the Gulf of Cadiz and emphasize particularly the first 100 km of the path where mixing was expected to be most intense. XCPs were obtained at sections A through F whenever a CTD cast indicated the presence of salty Mediterranean Water. CTD and XCP casts were considered concurrent if they were separated less than 1 nautical mile and 30 minutes.

The outflow survey was completed in five days. During this period several stations were occupied repeatedly in order to assess short timescale variability [section 2c(1)].

a. Data calibration and analysis

Water bottle samples were taken in regions of low salinity gradients and used to correct the Seabird conductivity measurements (Kennelly et al. 1989a). Salinity was calculated by Kennelly et al. (1989c) using the Seabird CTD pressure, temperature, and conductivity sensors and the method of Perkin and Lewis (1980). Potential temperature and potential density were calculated using EOS80. All temperatures described in this paper are potential temperatures referenced to the sea surface.

XCPs also measure temperature, which can be matched to CTD temperatures (Kennelly et al. 1989b). The XCP fall rate was then adjusted by comparing to concurrent CTD temperature profiles (Prater 1991). The CTD data were averaged over a 2-dbar interval for pressure, temperature, and salinity and the XCP data were averaged for pressure, temperature, and horizontal ve-

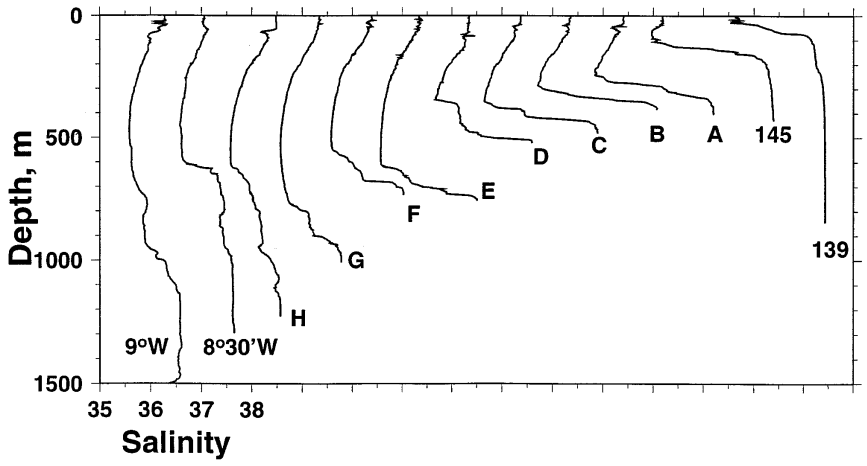

FIG. 3. Salinity profiles along the axis of the outflow, which we define as stations having the maximum salinity. Each profile is offset by a salinity of 1.0. Sections locations and station numbers are given in Fig. 2 (see also Prater and Sanford 1994).

locity. Some additional processing was required to remove questionable data points near the surface and to replace them with interpolated values. The surface values, particularly for the XCP profiles, were deemed unreliable because the probe had not fully adjusted to a uniform rotation rate. Hence, the 10-dbar value was used as a constant to the surface. The XCPs yield vertical profiles to within 2/3 dbar of the bottom with a vertical resolution of 1/3 dbar (Johnson et al. 1994a).

The XCP gives only the velocity shear and a reference velocity must be specified at some depth to determine the absolute velocity (Sanford 1971; Sanford et al. 1978), just as in geostrophic calculations. It has generally been assumed that the current vanishes at the depth of the salinity minimum (Ambar and Howe 1979a; Heezen and Johnson 1969; Hinrichsen et al. 1993). Typically in the Gulf of Cadiz, the salinity (temperature) decreases with depth within the North Atlantic Central Water (NACW) and then increases with depth within the Mediterranean outflow (Fig. 3). For instance, near section A the minimum salinity was subsurface and reached values of 36.0 psu just above the outflow (Fig. 1). Farther away from the strait where the outflow was deeper in the water column, the minimum salinity decreased to values less than 35.6 psu (Fig. 4). There was no water with salinity (and temperature) that low within the Strait of Gibraltar, and hence we have assumed that 1) the salinity minimum water must be motionless or moving toward the Mediterranean. To implement this as a reference level, the XCPs were adjusted so that the alongstream velocity at the base of the Atlantic layer, defined as the depth of the temperature minimum, was set to zero. Then we assumed that 2) the Mediterranean does not gain or lose salt, which requires that the net salt flux across each section must vanish. The integrated salt flux across each section was then calculated and a single reference velocity for each section was determined such that salt flux across each section was conserved (Baringer 1993). The resulting level of no motion found in this way was slightly deeper than the temperature minimum and varied in depth and σ_θ across the sections. We found that this referencing scheme nearly conserved mass and heat flux, and thus gave a more consistent result than was found using other reference levels, for example, a motionless salinity minimum.

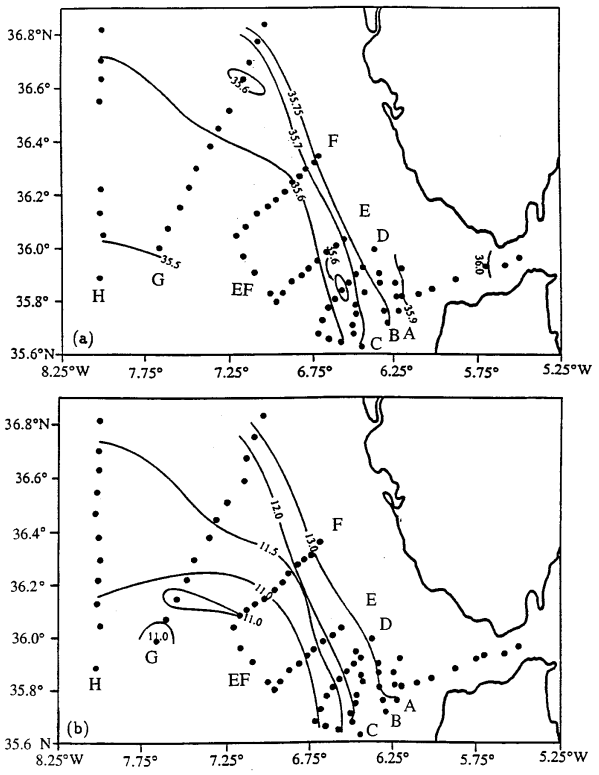

FIG. 4. Temperature and salinity of the NACW just above the outflow. (a) NACW salinity. (b) NACW potential temperature.

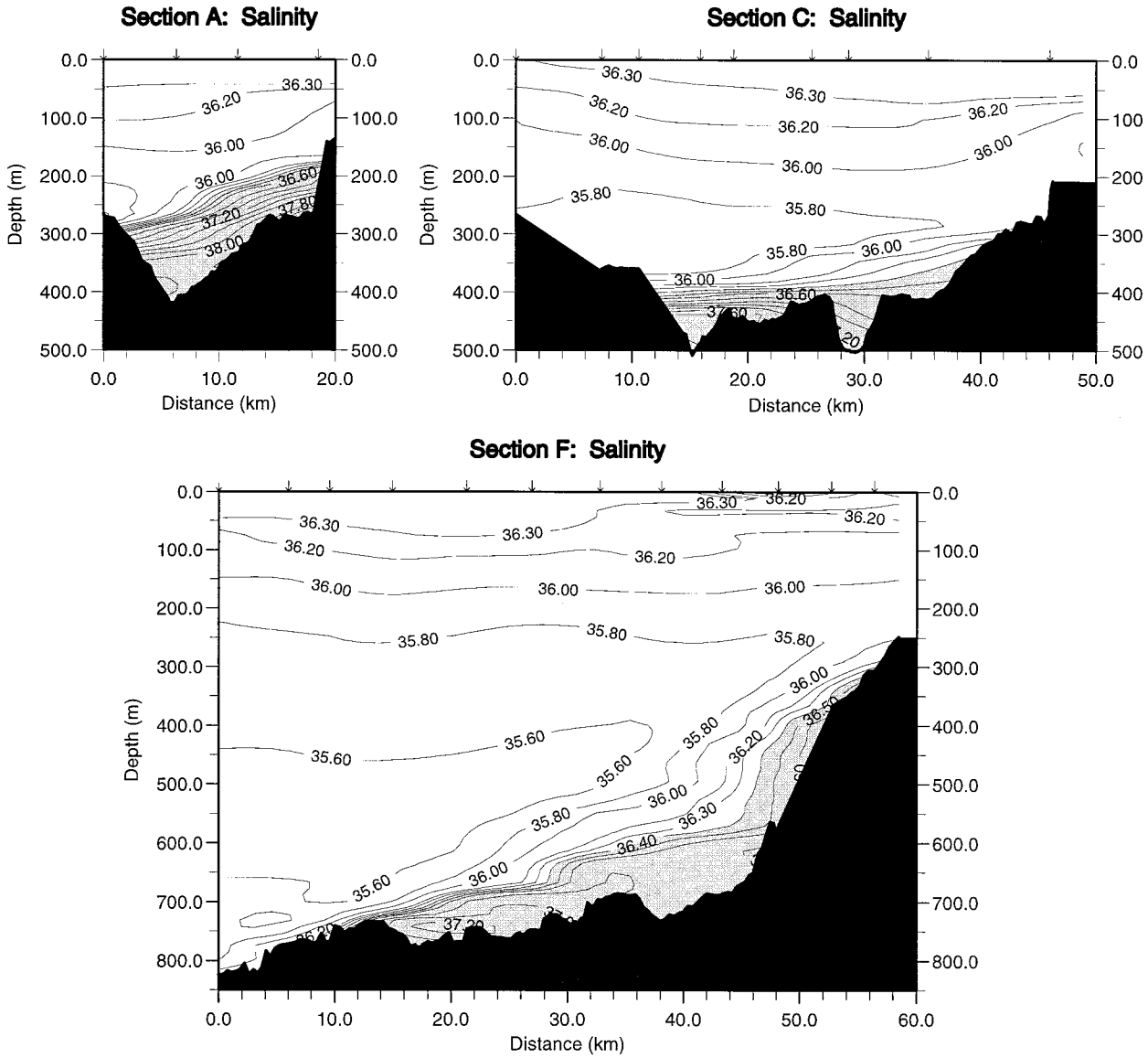

FIG. 5a. Salinity at sections A, C, and F. Vertical exaggeration 50:1. In all similar cross sections, the view is in the direction of the flow (i.e., north is to the right) and arrows mark the station locations. Salinity is contoured in 0.2 intervals except between 36.2 and 36.6 psu, which has 0.1 contour intervals. Values above 36.4 are shaded.

b. A first look at the observations

An alongstream salinity section has been made from the stations having the maximum salinity for each of the sections A–H and the alongstrait section I (Figs. 1, 3). Pure Mediterranean Water has salinity slightly greater than 38.4 psu and can be seen as a nearly uniform water mass that fills the deep Mediterranean Sea. The large density contrast between this water and the relatively fresh Atlantic water forces a reverse estuarine circulation in which the Mediterranean Water flows westward along the bottom under the eastward flowing North Atlantic water. As the Mediterranean Water spilled over the Spartel West Sill, it mixed with fresher North Atlantic Central water and continued down the continental slope. The outflow maintained a fairly constant thickness of about 100 m from section B to section E, where it began to thicken.

The eight sections oriented across the outflow all showed strongly sloping isohalines consistent with westward geostrophic flow (Fig. 5). A plan view of the outflow is given in Fig. 6 where the maximum salinity at each station is shown with its associated temperature, depth, and potential density. The temperature of the outflow at the Camarinal Sill was 12.9°C and the North Atlantic inflow ranged in temperature from 13° to 20°C (Fig. 5b). The outflow was initially nearly uniform in

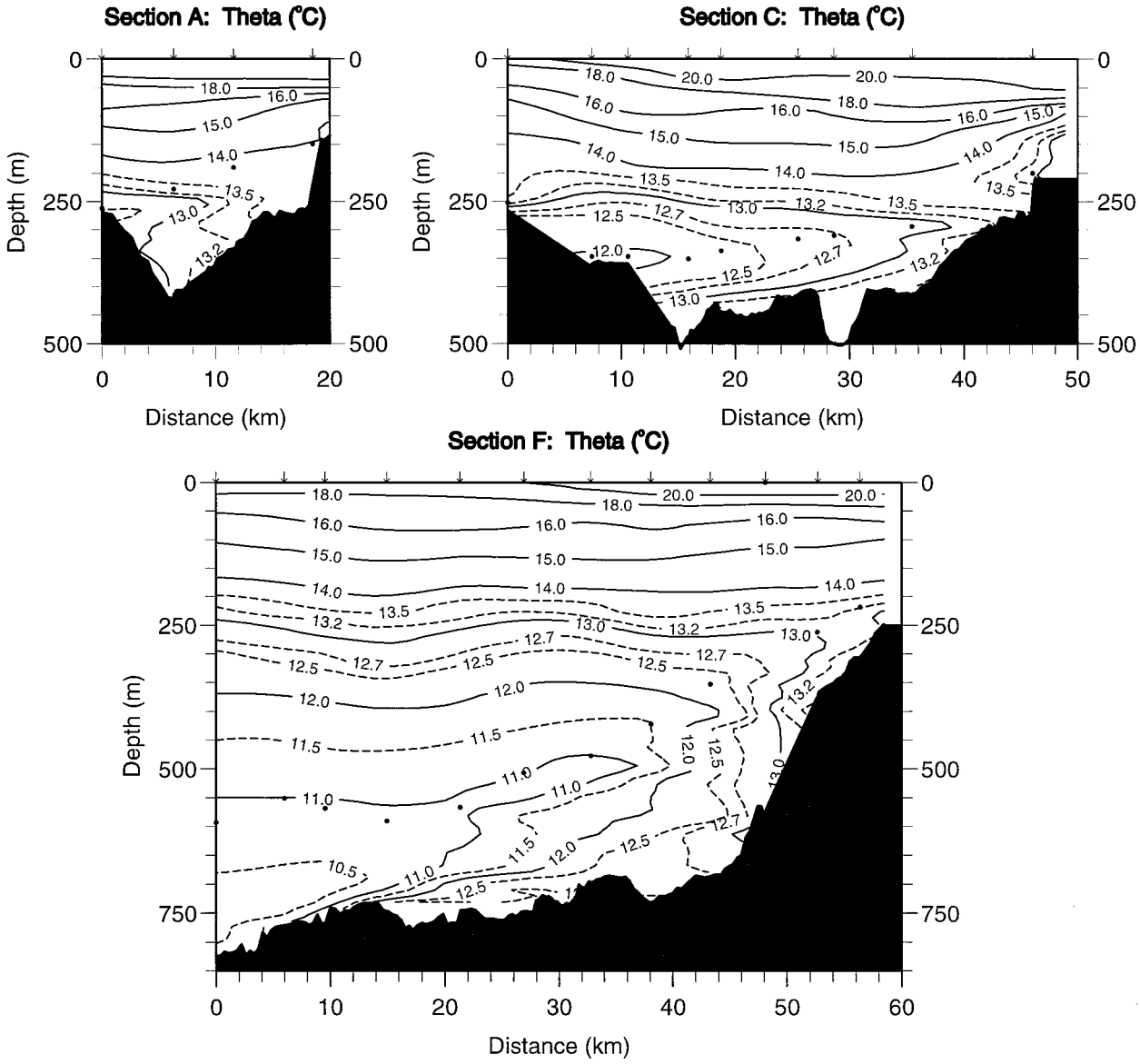

FIG. 5b. Potential temperature at sections A, C, and F. Dots represent the location of the salinity minimum at each station. Contour intervals are the same for each section.

temperature, and thus the salinity contours are good indicators of the isopycnal structure. In cross section (Fig. 5), the outflow looks as if it were a lens of dense water lying on the continental slope. Thus, from the strait until past section F, the outflow was a bottom-trapped density current (i.e., isopycnals greater than 27.6 kg m^{-3} intersected the bottom, Fig. 6). By about section G the deeper portion of the outflow began to detach from the bottom and the outflow began to intrude into the North Atlantic thermocline.

c. Time dependence

Our main goal in this paper is to describe the mean structure of the outflow. However, two aspects of time dependence are considered briefly here. Short timescale (especially tidal) variability would have been aliased into synoptic structure observed during the five-day survey, and thus would represent a significant sampling hazard. At minimum we attempt to estimate the magnitude of short timescale variability in the Gulf of Cadiz. At the other extreme, climate variations in the Mediterranean Sea could lead to variations in the outflow that might be detectable by a comparison with historical datasets, an issue also addressed in this section.

1) TIDAL VARIABILITY

Tidal fluctuations within the Strait of Gibraltar are very large (Bryden et al. 1989), particularly at the Ca-

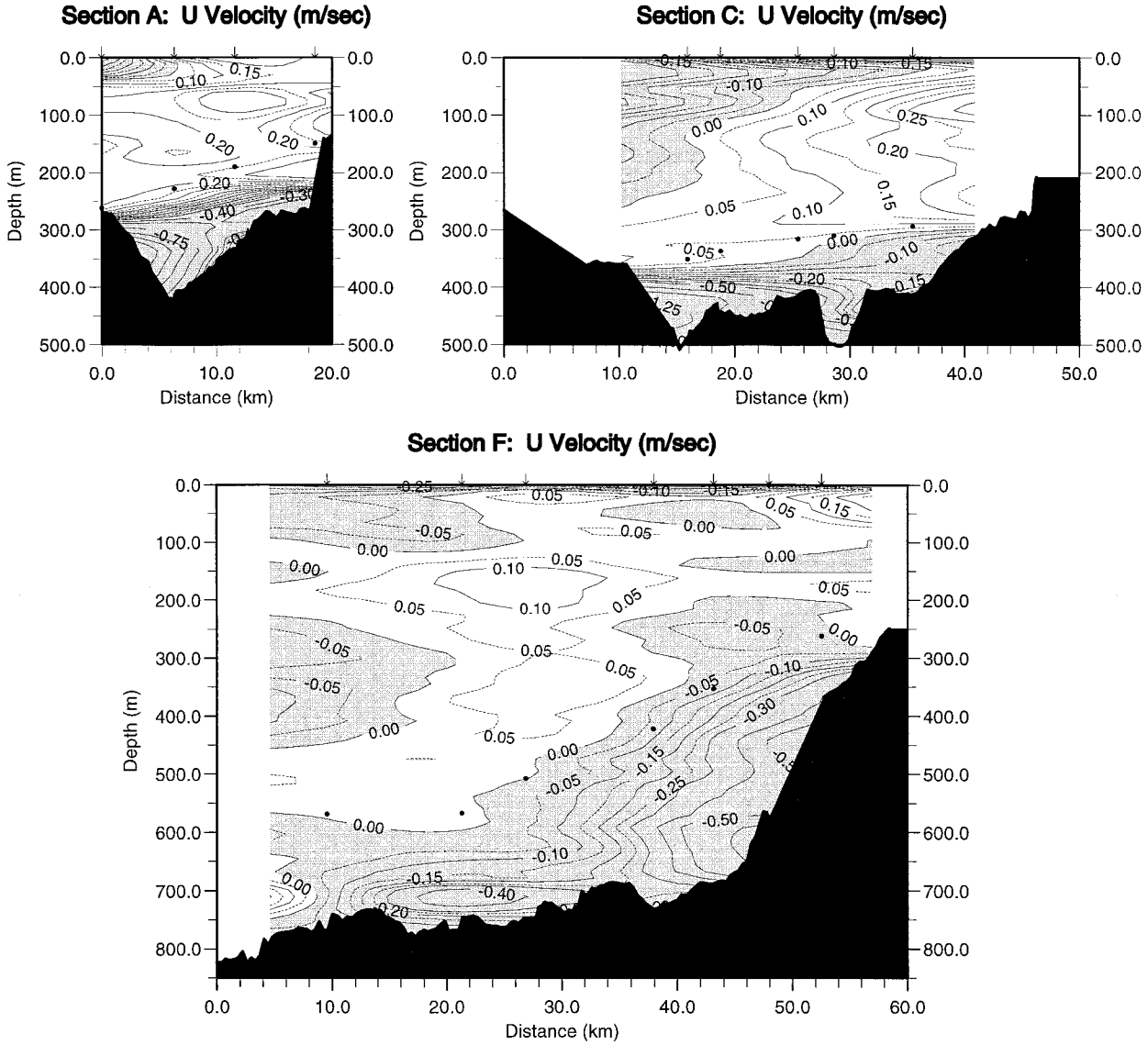

FIG. 5c. The component of XCP velocity normal to each section for sections A, C, and F. Velocity contoured in 0.05 m s^{-1} intervals above -0.3 m s^{-1}, 0.1 m s^{-1} intervals between -0.3 and -0.5 m s^{-1}, and 0.25 m s^{-1} intervals for speeds below -0.5 m s^{-1}. Velocity toward the west (negative or into the page) is shaded. Dots represent the location of the corresponding salinity minimum. As before, north is to the right.

marinal Sill (Fig. 1). Using current meters, the 1985–86 Gibraltar Experiment showed that the semidiurnal tide in the strait can reverse the flow at all depths and that the correlation between tidal transport and the vertical displacement of the 37.0 isohaline contributes half of the time-averaged outflow of Mediterranean Water (Bryden et al. 1994; Candela et al. 1989; Candela et al. 1990). Tidal variability decreases toward the west. Armi and Farmer (1988) found that the outflow has less than 20% tidal variation about a mean speed of 1.4 m s^{-1} at the Spartel West Sill (Armi and Farmer 1988). Candela et al. (1990) also found that the correlations between the outflow currents and interface depth drop to very small values away from the sill (Macdonald et al. 1993; Candela et al. 1990; Candela 1991). Therefore, although time-dependent fluctuations contribute significantly to the total mass, heat, and salt flux at the Camarinal Sill, their ''contribution to the mean fluxes (drops) to negligible values'' (Macdonald et al. 1993) to the west of the sill as the outflow enters the Gulf of Cadiz.

Our section A was located between the Spartel and Spartel West Sills where tidal variability may alias transport estimates (Armi and Farmer 1988). In section 4, we will find a larger transport and salt flux through section A than through other sections downstream, probably as a consequence of tidal aliasing. Transport calculations from section B and westward were internally consistent, suggesting little effect from tidal aliasing.

During the Gulf of Cadiz Expedition several stations were occupied repeatedly during a tidal cycle to observe

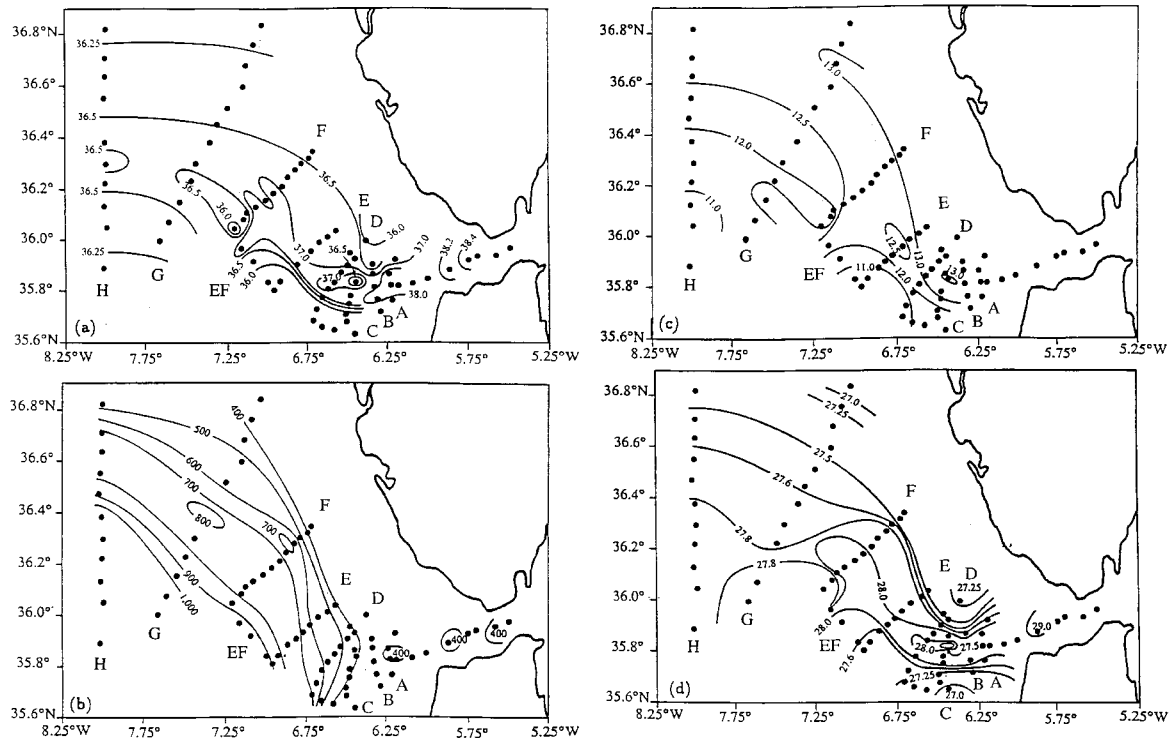

FIG. 6. Properties at the depth of maximum salinity at each station in the Gulf of Cadiz. (a: top left) The maximum salinity. (b: bottom left) The pressure at the maximum salinity. (c: top right) The potential temperature at the maximum salinity. (d: bottom right) Potential density at the maximum salinity referenced to the surface. Where no outflow is present, the bottom salinity and maximum pressure and the bottom potential temperature and potential density are plotted.

the short timescale variability of the outflow. For instance, at station 75 in section C (Fig. 6), a total of four CTD casts, six XCPs, and six XDPs were collected over a period of less than 2 days. The CTD casts showed a range in the maximum salinity of 37.9 to 38.2 psu. One profile exhibited layering in both temperature and salinity, while the other had a smooth gradient in properties through the same depth. The velocity profile was fairly steady, however, with a standard deviation of about 0.1 m s^{-1} (see also Johnson et al. 1994a). Even with this variability, there was little difference between the velocity-weighted average values of salinity (section 3) so that flux estimates are fairly insensitive to this tidal variability in the outflow (i.e., less than 10% maximum variation at this station).

Other variables may show more short timescale variability. The most dissimilar XDP profiles showed large dissipation values in the outflow layer with a relative minimum close to the depth of the velocity maximum (Lynch and Lueck 1989). However, there was an order of magnitude difference in average peak dissipation values in the outflow layer (10^{-1} vs 10^{-2} W m^{-3}). Note that higher-order moments like momentum and energy flux may be more sensitive to the tidal variability (Baringer and Price 1997; Baringer 1993).

2) MESOSCALE AND SEASONAL VARIABILITY

Mesoscale and seasonal variability can also alias any single outflow survey, which the observations presented here cannot address. The reader should consult Thorpe (1976) and Stanton (1983) for discussions of mesoscale variability. Our survey was made during the fall and there is some evidence in historical data of a weak annual cycle in transport with a minimum in fall (Bryden et al. 1989; Bryden et al. 1994; Ochoa and Bray 1991). Thus the transport estimates presented here may be a lower bound on the long term average.

3) A COMPARISON WITH HISTORICAL OBSERVATIONS

There have been at least six more or less complete hydrographic surveys of the Mediterranean outflow since the 1950s (Heezen and Johnson 1969; Madelain 1970; Zenk 1975a; Howe et al. 1974; Ambar and Howe 1979a; Ambar and Howe 1979b; Ochoa and Bray 1991). Over this period there has occurred a small but clearly detectable increase in the salinity of Western Mediterranean Intermediate Water (the outflow source water), about 0.05–0.10, due to man-induced reduction of river inflow into the Mediterranean Sea (Rohling and Bryden 1992). Our 1988 data showed that the salinity within the Inter-

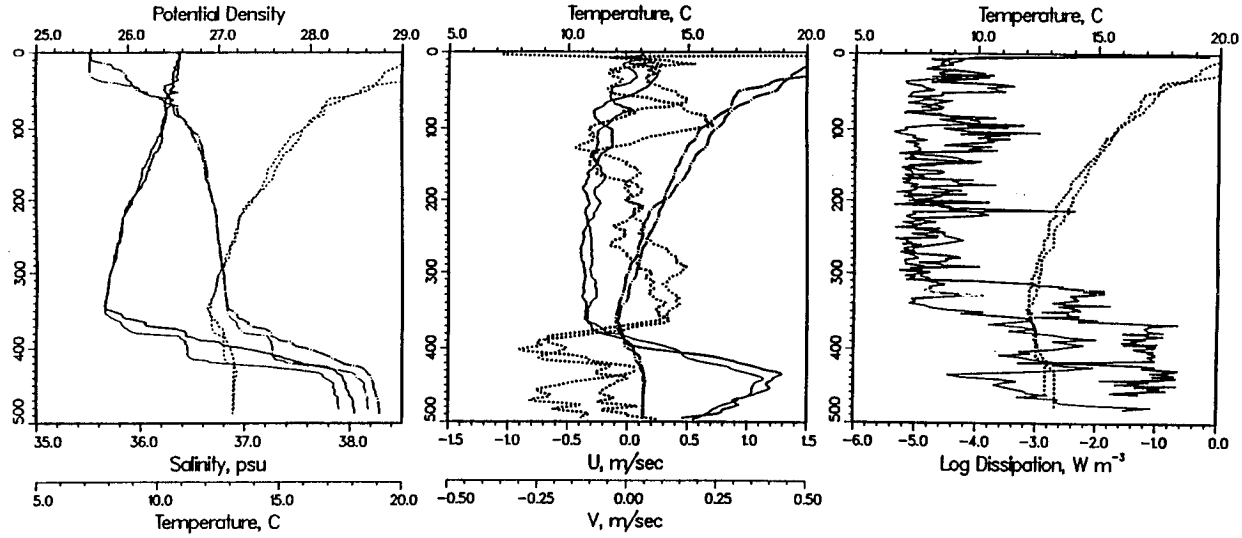

FIG. 7. Repeat occupations of station 75 (section C) that show the most dissimilar profiles. (a: left) CTD 75 and CTD 91 salinity (solid line), temperature (dashed line), potential density (chained line). (b: center) XCP 2544 and XCP 2556 projected into the direction of the maximum velocity; u is the downstream velocity (solid line), v is the cross-stream velocity (dashed line). The temperature from the XCPs is also shown (chained line). (c: right) XDP 704 and 804 dissipation (solid line) and temperature (dashed line). Note that the dissipation values differ by more than an order of magnitude in the outflow layer.

mediate Mediterranean Water just east of the entrance to the Strait of Gibraltar was 38.45 psu, which is about 0.04 greater than shown by Stommel et al. (1973), for example. Within the outflow proper, a precise comparison with historical data is made difficult by changes in measurement and navigation techniques combined with the small-scale and three-dimensional spatial structure of the outflow. As far as we can tell, the outflow observed in 1988 was very similar to that seen in the earlier surveys. For example, all of the surveys show that the Mediterranean Water flows along a path over the continental shelf and slope of the northern Gulf of Cadiz that has remained essentially unchanged. The thickness of the Mediterranean outflow layer and the core salinities that we observed are within about 20 m and 0.05 of those described by Heezen and Johnson (1969) and Madelain (1970) (i.e., indistinguishable given the horizontal variability, Fig. 8). Near Cape St. Vincent, where the outflow began to float off the bottom, the volume transport was largest within two modes whose core properties were $(\theta, S) = (12.17°C, 36.65$ psu) and (12.89°C, 36.43 psu) for the lower and upper cores respectively. These are within 0.2°C and 0.1 of the values quoted by Ambar and Howe (1979a) and within the scatter of the θ–S properties (more on this in section 4).

While hydrographic distributions appear to have remained appreciably constant, the reported estimates of the westward transport of Mediterranean water have decreased by at least a factor of 2, and our estimates of transport are evidently among the lowest yet. The first estimates of Mediterranean outflow transport by Nielson (1912) were made indirectly from estimates of the evaporation over the Mediterranean, then thought to be just over 1 m yr^{-1}, and observations of the inflow and outflow salinity at the Strait of Gibraltar. If a steady-state salt balance is assumed for the Mediterranean Sea, then these lead to inflow (eastward, upper-level flow) and outflow (westward, lower-layer flow) transports of 1.88 and 1.79 ($\times 10^6$ m^3 s^{-1}) respectively. In the decades that followed, this method has been updated with refined evaporation estimates (Sverdrup et al. 1942; Defant 1961; Bethoux 1979; Lacombe et al. 1981). The most widely quoted value is by Lacombe and Richez (1982), who estimated an exchange of 1.2×10^6 m^3 s^{-1}. Other similar estimates have ranged from 0.9×10^6 m^3 s^{-1} to 1.8×10^6 m^3 s^{-1} (summarized in Hopkins 1978). More recently, Bryden et al. (1989) have used current meter measurements from the Gibraltar Experiment to calculate a time-averaged outflow transport of 0.68×10^6 m^3 s^{-1} and an inflow transport of 0.72×10^6 m^3 s^{-1} (Bryden et al. 1994; Kinder and Bryden 1987). We are inclined to think that these are the most reliable estimates of the outflow transport within the strait because of their duration and because of their basis in direct current measurement. Our estimates of outflow transport at the western end of the strait are similar, 0.7×10^6 m^3 s^{-1}, of which about 0.4×10^6 m^3 s^{-1} was Mediterranean source water ($S \geq 38.4$) (more on this in section 4).

The time-mean transport of the outflow within the strait might now be regarded as fairly well known; however, the mixed transport within the Gulf of Cadiz is less so. Ambar and Howe (1979b) estimated an outflow transport of 1×10^6 m^3 s^{-1} near the Strait of Gibraltar, where some mixing has already occurred, and 3×10^6 m^3 s^{-1} near Cape St. Vincent. More recently, Ochoa and Bray (1991) estimated a net westward flux of Mediterranean Water of

0.5×10^6 m^3 s^{-1} near the strait and 2.2×10^6 m^3 s^{-1} near 7° 30′ W and 8°W (about halfway to the open North Atlantic). Using a mixing model of tracer data, Rhein and Hinrichsen (1993) concluded that the Mediterranean outflow transport reached a maximum near 8° W of 3.7×10^6 m^3 s^{-1} by assuming an outflow of 1×10^6 m^3 s^{-1} at the strait. All of these studies indicate that the transport of the (mixed) Mediterranean outflow increases by a factor of about 3 somewhere in the Gulf of Cadiz, but where and why has not been well defined in the hydrographic surveys reported to date.

3. Descent and spreading along the continental slope

The Mediterranean outflow water descended into the Gulf of Cadiz and spread out over the northern continental shelf and slope (Figs. 6 and 9). By section H, approximately 240 km downstream, some of the outflow water had descended almost 1 km, and the width had grown to about 80 km. This descent and spreading of the outflow appear to be related phenomena.

Around sections A and B the outflow was confined within a channel on the continental shelf that was about 12 km wide (Figs. 5 and 8) and appears to be an extension of the subsurface topography of the Strait of Gibraltar. At section C, which was close to the shelf-slope break, the topography could still be characterized as a channel, though it had broadened to about 24 km. Note that there is a ridge that runs roughly parallel to the outflow current at section C (Fig. 5), whose height was a little more than half the thickness of the outflow. This topographic feature appears to have split the outflow into two partially connected branches at section C. Other topographic features farther downstream also appear to have steered the outflow into two main branches (as emphasized especially by Zenk 1975a), which then acquired somewhat different θ–S characteristics on account of entrainment of different North Atlantic Central Water (described further in section 4).

Westward of section C, the topography fans out and the outflow was free to spread out as it descended the continental slope. The northern or onshore side of the outflow descended from about 180 m at section A to about 300 m at section F; the southern or offshore side descended from about 400 m at section A to about 750 m at section F (Fig. 8). Still farther west, near Cape St. Vincent, the onshore and offshore sides had descended to about 450 m and 1450 m respectively (where the sides are defined by the minimum and maximum depth of salinity anomalies greater than 0.5). Thus, the descent of the outflow was highly asymmetric and was due almost entirely to the descent of the southern, offshore side. Given that the outflow was on a fairly uniform slope and its width increased from about 12 km to about 80 km westward from section A to F, some sort of asymmetry was inevitable.

Spreading could occur by a depth-dependent process,

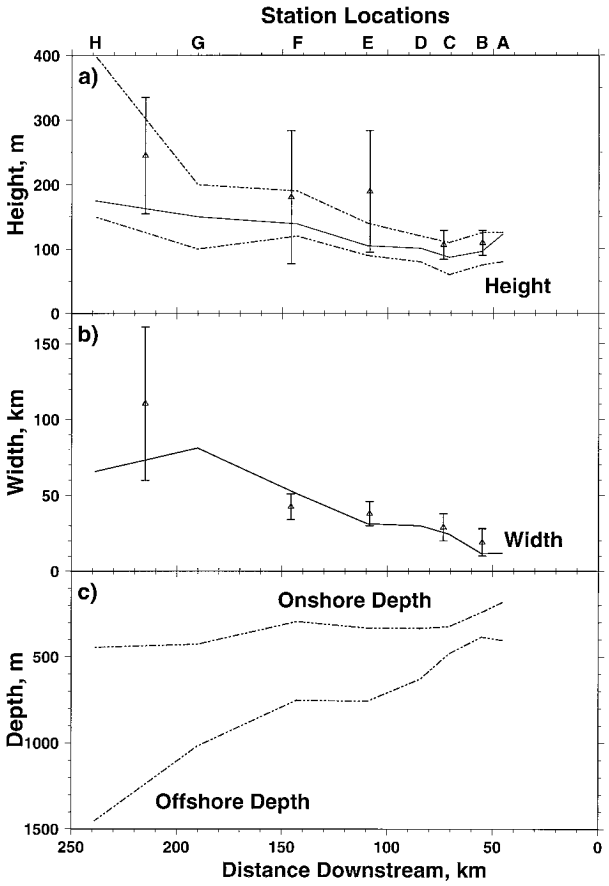

FIG. 8. Height, width, and depth of the Mediterranean outflow. (a) The height (solid line) was determined from the area of outflow (i.e., the area of the water moving westward) divided by the width. The chained lines show upper and lower bounds on the height estimated from the sections shown in Baringer (1993). The vertical bars (triangles) represent similar height ranges taken from Smith (1975) and Madelain (1970). (b) The width (solid line) is defined as the distance between stations with high salinity outflow water plus half the distance to adjacent stations (equivalently, the outflow width could be defined by using any salinity value between 36.25 and 36.4). The vertical bars (triangles) represent similar width ranges taken from Smith (1975) and Madelain (1970). (c) The bottom panel shows the depth of the onshore and offshore edge of the outflow defined as the minimum and maximum depth where the salinity anomaly exceeds 0.5 (i.e., the outflow salinity exceeds the background salinity). The distance downstream is the distance from the Camarinal Sill.

due say to the secondary circulation associated with Ekman veering, or by a depth-independent process, which could also be associated with bottom frictional effects provided the frictional effects were stronger on one side of the outflow than the other. The XCP current measurements make it possible to describe the kinematics of spreading and the XDP measurements and analysis of Johnson et al. (1994a) make it possible to describe the the horizontal variation of bottom stress.

a. Spreading by Ekman veering

Ekman veering within the outflow would be expected to produce a secondary circulation in which lighter wa-

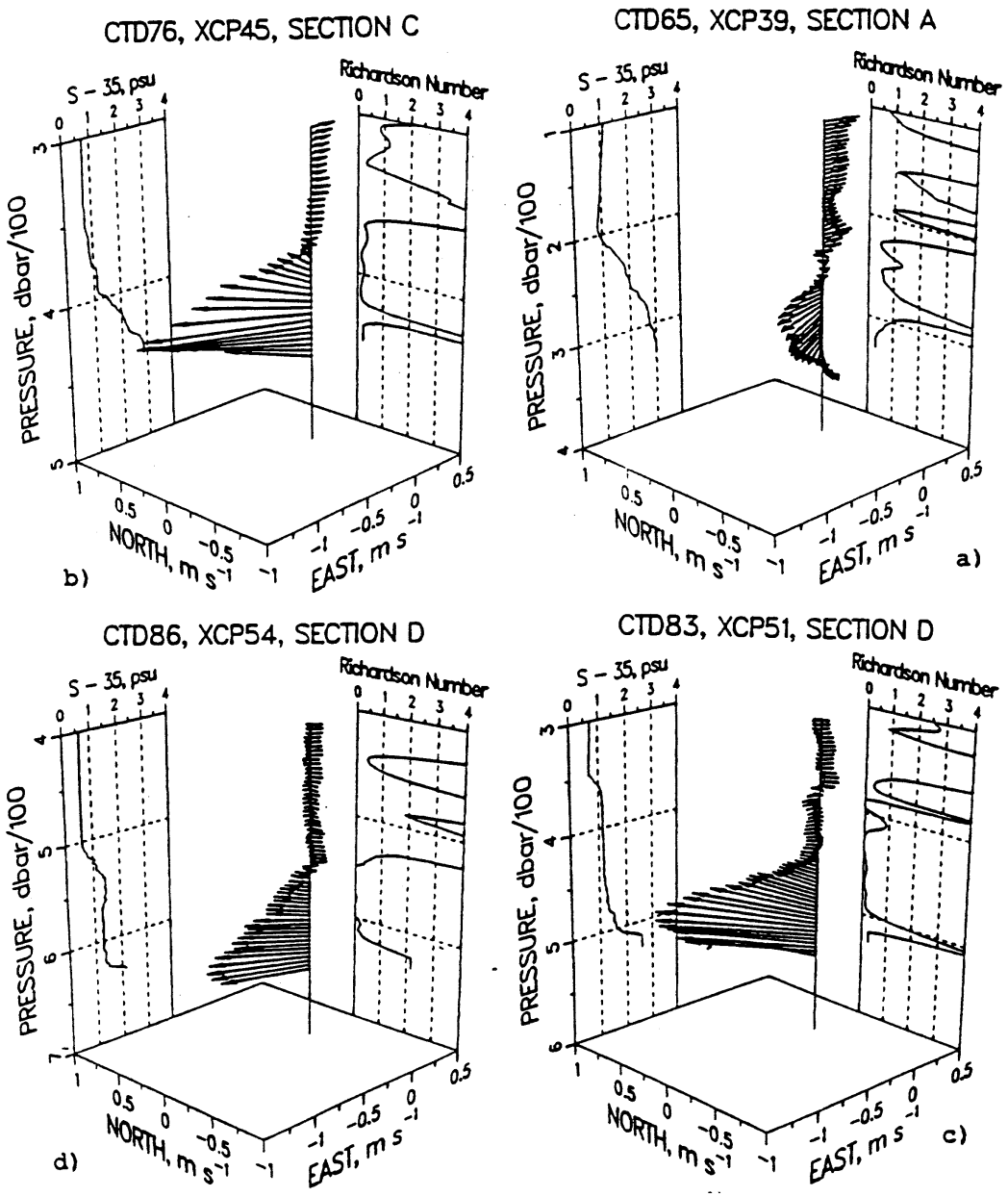

FIG. 9. Three-dimensional velocity for CTD/XCP drop pairs. The XCP velocity profiles are plotted at 4-m intervals. Salinity anomaly and gradient Richardson number are plotted in side panels. Notice that the velocity profile usually spirals with depth in the Ekman sense. (a) Upper right panel. CTD 65 contains salty Mediterranean Water below 200 dbar moving toward the SW. Low gradient Richardson numbers (Ri) are found in the interface between 225 and 270 dbar and in the well-mixed bottom layer. Large values of Ri occur at the velocity maximum near 285 dbar. (b) CTD 76 contains Mediterranean Water moving toward the NW. There were very low gradient Richardson numbers through the interface layer from 370 dbar down to the velocity maximum at 425 dbar. (c) CTD 83 is an example of the layered structure of the outflow. (d) CTD 86 has an unstable density profile suggesting mixing.

ter within the interface would flow toward the right (looking in the direction of the flow) or upslope, while denser water at the bottom of the outflow would be drained off in a bottom Ekman layer moving to the left, or downslope [Johnson and Sanford (1992) describe this secondary circulation within the Faroe Bank Channel outflow].

Each of the velocity profiles shown in Fig. 9 exhibits veering of the velocity profile through the transition layer between the westward flowing Mediterranean Water and the North Atlantic Central Water above. Examination of the velocity at 10 m and 40 m above the bottom also reveals this veering (Fig. 10). Stations within the westward moving outflow generally had the deep-

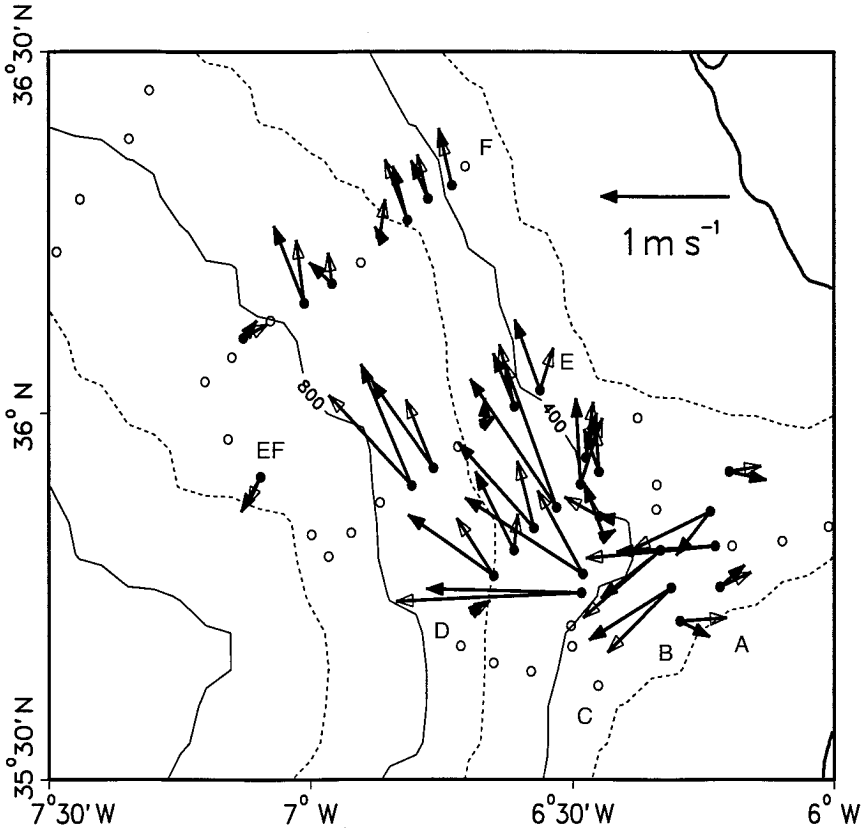

FIG. 10. XCP measured velocity at 10 dbar (solid arrow heads) and 40 dbar (open arrow heads) above the bottom. Open dots indicate stations where no XCP was dropped.

er velocity directed downslope relative to the current 40 m above the bottom. Three exceptions are noted, all of which were located at the southernmost stations along sections B, C, and E. In all three cases we believe that the outflow was diverted by local bathymetric features; at sections B and C the outflow was in a channel as noted previously and, at section E, this station was in a slight depression. The full XCP profiles, a few of which are shown in Fig. 9, also showed veering in the interfacial boundary layer that appears to be consistent with Ekman dynamics. This veering was generally larger than that in the bottom boundary layer.

To quantify the veering, we divided the outflow into two layers, defined to be above and below the velocity maximum. An ensemble average of the angle between the average velocity *above* the velocity maximum and the velocity maximum itself gave an angle of $5.3 \pm 0.4°$ ($\pm$ the standard error, positive means to the north relative to the velocity maximum). The average angle below the velocity maximum was $-2.8 \pm 0.3°$ (negative means to the south or counterclockwise with depth). The average angle between the upper and lower portions of the outflow was thus about 8°. This implies a spreading rate of 0.14, over 100 km downstream, the width would increase by about 14 km due to this depth-dependent spreading process. This is considerably smaller than the spreading rate actually observed, roughly 0.5.

b. Depth-independent spreading

To evaluate the depth-independent spreading, we have mapped the vertically averaged velocity at each station containing outflow (Fig. 11). The direction of the averaged velocity at the northernmost and southernmost stations containing outflow was then differenced to evaluate the depth-independent spreading. At section C, the difference in direction was 50°, and divergent. At section D the average angle was 34°. Farther downstream, the angle was smaller. These large spreading angles are about the right magnitude to account for the observed spreading.

Thermal wind effects acting together with bottom friction could help generate such a divergent flow (Ezer and Weatherly 1991). To see how, it is helpful to imagine that the outflow is, in cross section, a lens of dense stratified water sitting on a bottom that slopes uniformly up toward the north (as in Baringer and Price 1997, their Fig. 5). Averaged across the lens, isopycnals must have a north–south slope that is the same as the bottom slope. Assuming that the lens is stratified, then the ther-

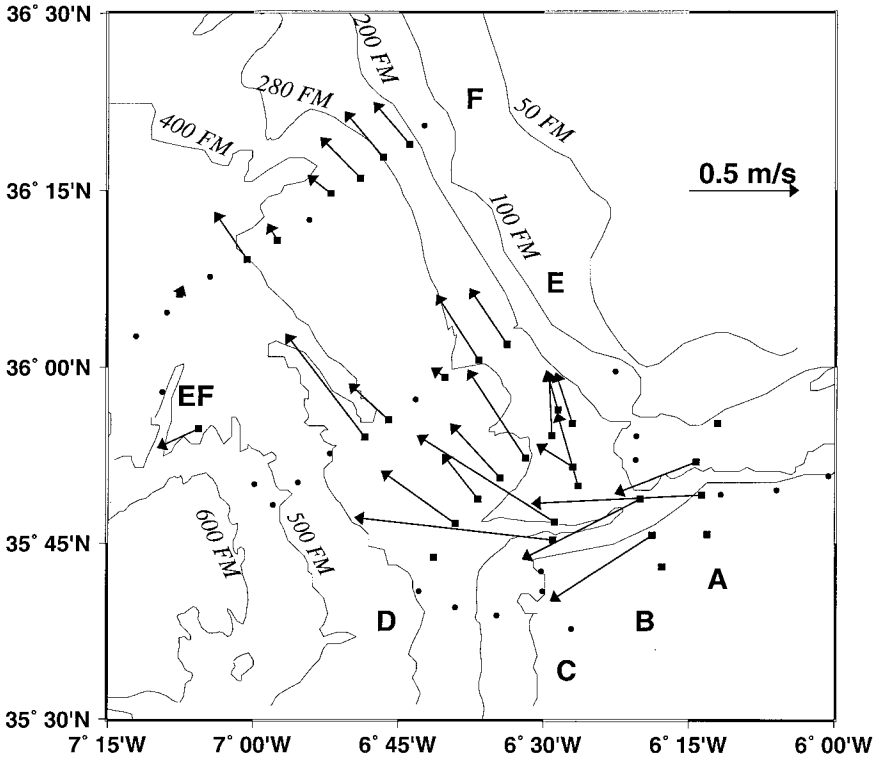

FIG. 11. Vertically averaged XCP velocity of the outflow. Stations with an XCP are marked with a square (stations with no outflow have no arrows). Stations without an XCP (i.e., CTD only) are marked with a circle.

mal wind will be an increasingly westward current with depth that depends on the slope of the isopycnals and the stratification. The local isopycnal slope will, of course, vary across the lens; there will likely be a reduced north–south slope on the north or shallow side of the outflow (which is evident in most of the sections of Fig. 5) and an increased north–south slope on the south or deep side (this is not evident, perhaps in part due to bottom slope variations). The trend in isopycnal slopes coupled with generally stronger stratification observed in the offshore, deeper stations (most sections show this pinching of isopycnals on the offshore side) leads to a stronger (weaker) westward bottom current on the south (north) side of the outflow. This was observed at five of the six sections A–F but not at D (Fig. 10). Assuming that larger near-bottom velocities cause larger bottom stress, then larger stresses would be expected on the offshore side, as indeed observed by Johnson et al. (1994b). Baringer and Price (1997) show that bottom stress allows or causes the outflow to descend topography and hence the offshore side should descend deeper due to the increased bottom stress.

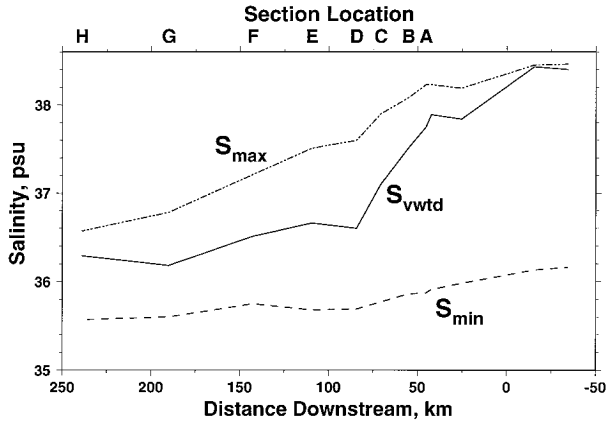

FIG. 12. Salinity versus downstream distance. The maximum salinity across each section (the chain dashed line, S_{max}) gradually decays downstream, while the velocity-weighted salinity (the solid line, S_{vwtd} decays rapidly within the first 40 km beyond section A. The dotted line S_{min} is the salinity of the overlying North Atlantic Central Water.

4. Mixing and entrainment of North Atlantic Central Water

The downstream evolution of the Mediterranean outflow can be characterized by the downstream decrease of salinity. In doing this, it is helpful to represent the salinity by a single value. This salinity has sometimes been taken to be the core value, the maximum value of salinity found in a transverse section (Heezen and Johnson 1969) (Figs. 3, 6, 12). The core salinity decreases

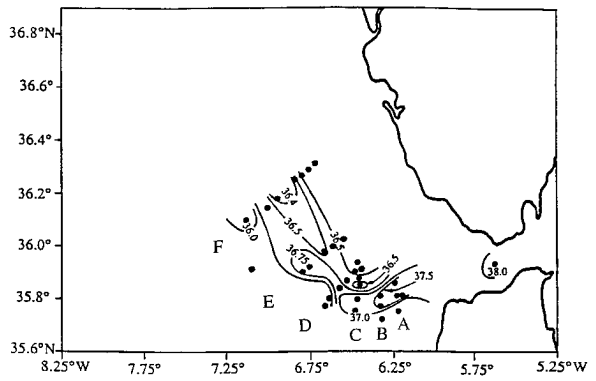

FIG. 13. Velocity-weighted salinity, as defined in (1), at stations where XCP/CTD data were available and where there was an outflow. The velocity-weighted salinity shows the two dominant transport modes separating at section E and F.

downstream at a fairly steady rate, leading to the inference of gradual mixing along the path (Heezen and Johnson 1969). Our observations showed that the core salinity was almost always very close to the bottom and often in water that was moving very slowly. Consequently, the core salinity does not appear to be the most apt single value to characterize the salinity of the outflow (as expanded upon below).

To make a more representative single or averaged value, we have combined the salinity and XCP velocity to estimate a velocity weighted salinity S_{vwtd} at each station as

$$S_{\text{vwtd}} = \frac{\int_D^{D+h} S\mathbf{v}\cdot\mathbf{n}\, dz}{\int_D^{D+h} \mathbf{v}\cdot\mathbf{n}\, dz}, \tag{1}$$

where **n** is normal to each section (Fig. 13). This is the equivalent salinity of a single layer moving with the average velocity, preserving the observed volume and salinity flux at each station. This velocity-weighted salinity was calculated only at CTD stations with concurrent XCP profiles. To average over the entire outflow on a given section, we estimate the transport-weighted salinity $\bar{S}$ as

$$\bar{S} = \frac{\int_0^W \int_D^{D+h} S\mathbf{v}\cdot\mathbf{n}\, dz\, dy}{\int_0^W \int_D^{D+h} \mathbf{v}\cdot\mathbf{n}\, dz\, dy}, \tag{2}$$

where $D(x, y)$ is the bottom depth, $h(x, y)$ the top of the outflow, and $W(x)$ the width of the outflow defined in Fig. 8. Figure 12 illustrates $\bar{S}$ at each section as a function of downstream distance. Here $\bar{S}$ decreased downstream from 37.8 to 36.7 psu in the 40 km from section A to D. The greatest change occurred between sections C and D, suggesting especially intense localized mixing with fresher, overlying NACW between those sections.

The mixing between the Mediterranean outflow and NACW appears to be an entrainment process in so far as the transport of the westward moving (mixed) Mediterranean water increases more or less in proportion to the salinity decrease. The transport for each section was calculated using the referenced XCP velocities described in section 2a and by assuming that the outflow was entirely bottom trapped, reaching a width shown in Fig. 8, and capped by water at the temperature minimum moving into the Mediterranean. Where the outflow was separated from the bottom at sections G and H, this transport estimate includes everything moving westward below the reference [i.e., the eastward-flowing Mediterranean undercurrent first described by Ambar and Howe (1979b), which we found at section H was not included].

These transport estimates (Table 1) indicate an increase from 0.7 to 1.2 ($\times 10^6$ m^3 s^{-1}) between sections B and D, and a similar increase between sections E and F. Thus, the transport doubled by section F, or within about 140 km of the Camarinal Sill. This increase in transport downstream is similar for other reference levels and also for geostrophic transport estimates, indicating that the estimated entrainment is insensitive to the reference level chosen.

We can use conservation of salt to estimate the flux of pure Mediterranean water Q_{Med} and the entrained NACW, Q_{ent}:

$$\bar{S}Q_{\text{out}} = S_{\text{Med}}Q_{\text{Med}} + S_{\text{NA}}Q_{\text{ent}}, \tag{3}$$

where $\bar{S}$ is the transport-weighted salinity defined above, and S_{Med} and S_{NA} are the Mediterranean and NACW salinities taken as the constants 38.4 and 35.6 psu. This can be combined with conservation of mass and rewritten as

$$Q_{\text{Med}} = \left[\frac{\bar{S} - S_{\text{NA}}}{S_{\text{Med}} - S_{\text{NA}}}\right] Q_{\text{out}}, \tag{4}$$

where the total transport Q_{out} is the sum of Q_{Med} and Q_{ent}. These latter two transports were then estimated from Q_{out} and $\bar{S}$ as calculated from observations (Table 1). The inferred flux of pure Mediterranean Water was 0.4×10^6 m^3 s^{-1} except at section F, where it was slightly higher, and at section A, where it was 0.68×10^6 m^3 s^{-1} and most likely effected by tidal aliasing. Aside from section A, it appears that the flux of pure Mediterranean Water was approximately conserved and that the transport increase was consistent with the decrease in the velocity-weighted salinity. This too indicates that the entrainment occurred primarily between sections C and D and also between sections E and F. As we noted in section 2c(2), this estimate of pure Mediterranean Water is much lower than historical estimates (Lacombe and Tchernia 1960; Ambar and Howe 1979a) but is consis-

TABLE 1. Observed and estimated transports for each section: Q_{out} is the observed total outflow transport. The transport of pure Mediterranean Water Q_{Med} is determined through a simple mixing argument, Eq. (4), assuming that the Mediterranean and NACW salinities, S_{Med} and S_{NA}, are the constants 38.4 and 35.6 psu, respectively. Q_{ent} is the estimate of entrained NACW [i.e., the denominator of equation (2)], and $\bar{S}$ is the observed transport-weighted salinity defined in (2). Note that section "F + FE" is a combination of transport from section F and section FE. Assuming a fixed Q_{Med} of 0.4 m^3 s^{-1}, a spatially variable S_{NA} can be estimated from the observed transports and salinities. Note that S_{NA} shows similar spatial variability as the salinity just above the outflow (Figs. 11 and 15). Similarly, assuming Q_{Med} = 0.4 m^3 s^{-1} and S_{NA} as just determined, a new total outflow transport Q_{new} can be estimated that exactly conserves salt flux through all the sections. All of these transport estimates indicate a localized entrainment between sections C and D and also between sections E and F.

					Q_{Med} = 0.4 × 10^6 m^3 s^{-1}			
Section	Q_{out}	Q_{Med}	Q_{ent}	$\bar{S}$	S_{NA}	Q_{ent}	Q_{new}	Q_{ent}
A	0.88	0.68	0.20	37.75	37.2	0.48	0.52	0.12
B	0.65	0.44	0.21	37.51	36.1	0.25	0.61	0.21
C	0.74	0.40	0.34	37.10	35.6	0.34	0.74	0.34
D	1.04	0.37	0.67	36.60	35.5	0.64	1.07	0.67
E	1.07	0.40	0.67	36.65	35.6	0.67	1.05	0.65
F	1.40	0.47	0.93	36.54	35.8	1.00	1.19	0.79
F + FE	1.53	0.50	1.03	36.51	35.8	1.13	1.23	0.83

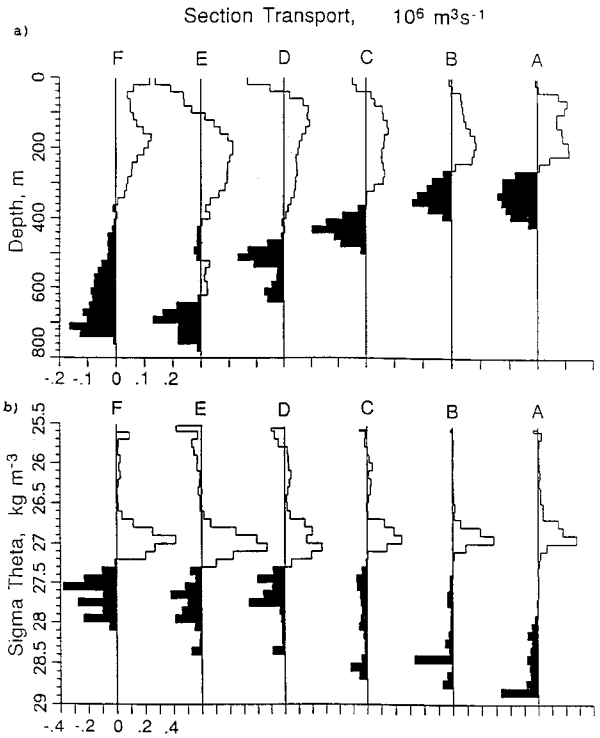

FIG. 14. Transport of water in σ_θ and depth classes for each section (Baringer 1993; Price et al. 1993). The total outflow transport is listed in Table 1. (a) Transport in depth bins. (b) Transport in σ_θ bins. The outflow (or westward) transport is shaded. The eastward transport is unshaded and is largest at middepth (at some sections the near-surface layer is moving westward but is left unshaded).

tent with the more recent estimates of Ochoa and Bray (1991) and Bryden et al. (1994).

Note that this simple mixing argument requires that the outflow is steady and that S_{NA} is constant. However, Figs. 4 and 12 show that S_{NA} increased toward the Strait of Gibraltar. We can solve for variable S_{NA} by fixing Q_{Med} and rewriting (3) (Table 1). This modified entrainment estimate still supports the localized increases in transport between sections C and D and also between sections E and F. Similarly, we could acknowledge undersampling at section A and rewrite (4) to solve for a new transport estimate Q_{new} that exactly conserves salt flux through all the sections. This new estimate reduces the transport at section A and section F but still requires intense localized mixing (Table 1), which thus appears to be a robust result.

a. Transport profiles

Some other important features of the mixing process can better be seen by an analysis of the transport profiles, where both depth and density are useful as the vertical coordinate. Figure 14a illustrates the former, where the transport at each section is averaged into 20-m depth intervals. Figure 14b illustrates the transport averaged into 0.1 kg m^{-3} σ_θ intervals. This presentation suggests that the path of the outflow has three major parts: a nearly constant depth interval between sections A and B, a region of steep descent between sections B and E, and a nearly constant depth between sections E and F (we know from hydrography that there is a continued gradual descent farther downstream, Fig. 1).

Along the first part, between sections A and B, the outflow mixes very little with the overlying NACW, as evidenced by the nearly constant transport (see Q_{ent} of Table 1). It does appear to mix internally, as suggested by the decrease of both the maximum salinity and the velocity-weighted salinity (Fig. 12). At section A, the transport was concentrated in the highest σ_θ class, whose density was almost that of pure Mediterranean Water. As the outflow moved to section B, the maximum transport appeared in a slightly lighter density class suggesting internal mixing. A similar change occurred from section B to C, with the transport more evenly distributed in density (Fig. 14). At section A, there is little water in the density range from 27.3 to 28.0 σ_θ, but by section C the transport in this density class had increased considerably, even though the total transport remained similar. This pattern suggests internal mixing that eroded the maximum density and salinity without substantial entrainment of NACW.

Along the path from section C to F, the outflow descended from 500 m to 800 m in only 40 km. In this region, $\bar{S}$ decreased most rapidly (Fig. 13), as noted before, and the transport increased by 0.33 × 10^6 m^3 s^{-1} due to entrainment of NACW. Most of this transport increase appeared in the 27.3–28.0 density range, which is characteristic of mixed Mediterranean Water. At section A, only 0.03 × 10^6 m^3 s^{-1} of this density range

was present, but by section F the majority of the outflow transport, 1.3×10^6 m^3 s^{-1}, was in this density range.

The eastward flowing NACW showed corresponding changes in its transport. The eastward transport was mostly in the 26.6–27.3 σ_θ range just above the outflow, which changed significantly as the flow moved east from section F to section A. This density range had 0.5×10^6 m^3 s^{-1} flowing east through section D and was greatly reduced, down to 0.15×10^6 m^3 s^{-1}, at section C. This convergence of the eastward transport is consistent with the amount required to supply the entrainment into the outflow.

Along the third part west of section E, the outflow gradually descended from 800 m to 1400 m over a distance of about 200 km (the center of mass descended from 609 m to 673 m between sections E and F even though the maximum depth appears to be nearly constant in Fig. 14a). Over this region there was little further decrease in S, though the transport increased by 0.4×10^6 m^3 s^{-1} between sections E and F.

b. Horizontal temperature and salinity variations

As the outflow progressed downstream, the density range of the outflow narrowed somewhat from 27.6–28.9 σ_θ at section A to 27.3–28.1 σ_θ at section F. What is not clear from Fig. 14 is that most of this density variation at section A was due to vertical stratification, while at section F the density variation was due in a large part to horizontal variation. The θ–S structure also varied significantly along the path of the outflow. The outflow exited the strait with a fairly narrow θ–S relationship, which broadened considerably as the outflow moved farther downstream (Figs. 6 and 15). We attribute this increase in the θ–S envelope to local mixing with NACW having different properties.

Near the strait, the temperature of the outflow at the salinity maximum was fairly uniform, varying from 13.1° to 13.3°C (Figs. 6 and 15a). Farther downstream, this temperature difference increased and by section F was 12.5°–13.0°C. Even larger temperature differences were observed farther west. Notice that the outflow was warmer on the north side, which was also the shallower side.

The NACW just above the outflow maintained a tight θ–S relationship throughout the Gulf of Cadiz (Figs. 15 and 16) including section D where the potential temperature at the salinity minimum varied by 2.0°C across the outflow. The NACW just above the outflow was always warmer, saltier, and less dense toward the northern, shallower stations. This difference in the θ–S properties of the NACW was simply a manifestation of the vertical stratification of the NACW and the sloping interface of the outflow. The θ–S relationship within the outflow was fairly linear, which suggests local mixing between the outflow with the NACW directly above it. Thus, the horizontal variations in outflow θ–S arose through local mixing with different NACW: the shallower, northern side of the outflow mixed with warmer NACW than did the deeper offshore side and consequently became warmer than the offshore side.

c. A remark on modes and cores

A significant by-product of this spreading and mixing process is the development of two preferred transport modes having fairly distinct θ–S properties (Seidler 1968; Ambar 1983). These modes (which are more often called cores) have been noted by all previous investigators and were emphasized particularly by Ambar and Howe (1979a) and Zenk (1975b). Near Cape St. Vincent the modes may become sufficiently separated vertically and horizontally to form two separate subsurface salinity maxima (and thus the phrase ''cores''), tending to settle around 750 m and 1300 m along the 27.5 and 27.8 σ_θ surfaces. These modes persist as identifiable features for a very long distance downstream and can be found within the submesoscale eddies of Mediterranean Water found in the open North Atlantic (Zenk 1970; Armi and Zenk 1984). [Ambar and Howe (1979b) also identified a third, shallower mode near 7°W between 400 and 600 m (Zenk 1975a) along the coast of Portugal (Ambar 1983) that was thought to originate from winter mixed layers on the northern shelf in the Gulf of Cadiz (Ambar and Howe 1979b).]

We noted previously that the outflow had a very narrow θ–S range where it entered the Gulf of Cadiz, compared to the difference in θ–S between the two cores found downstream in the western Gulf of Cadiz (Table 2). Thus, the difference in θ–S properties between the modes must have originated within the Gulf of Cadiz as the outflow spread out and mixed with the stratified NACW. This was also suggested by Ambar and Howe (1979a).

The first clear evidence of two cores occurred at section E where the upper mode had maximum XCP speeds in excess of 0.4 m s^{-1}, while the lower mode centered at 750-m depth had XCP speeds greater than 0.6 m s^{-1} (Fig. 11). There was no clear separation of the salinity into modes, but the velocity field showed a distinct minimum speed of about 0.1 m s^{-1} between the two velocity maxima at section F (Fig. 5c). The velocity-weighted salinity shows the two modes clearly (Fig. 13).

The upper mode descended from about 500 to 800 m in the Gulf of Cadiz while it mixed with warmer NACW (Ambar and Howe 1979a). Much of the transport increase between sections E and F occurred due to a doubling of the transport in the upper core from 0.39×10^6 m^3 s^{-1} to 0.95×10^6 m^3 s^{-1}. The lower mode descended from 500 m to over 1300 m in the same area and thus mixed with colder NACW (Fig. 15b).

5. Mixing processes

The mixing processes that modified the Mediterranean outflow water appear to be of two kinds. There is clear

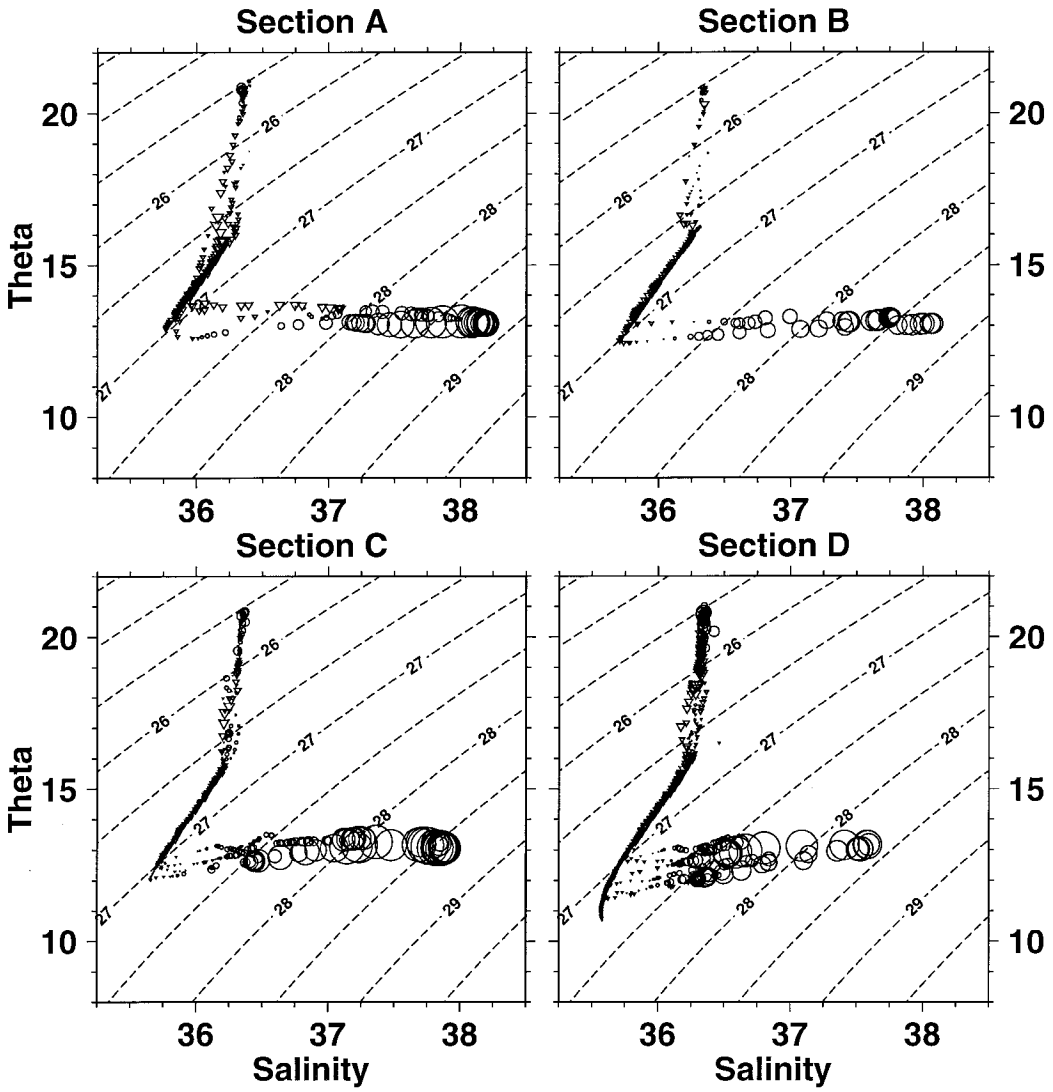

FIG. 15a. Potential temperature versus salinity for sections A, B, C, and D. For stations with concurrent CTD/XCP profiles, westward flow (circular symbols) and eastward flow (triangular symbols) are plotted for every 4 dbar of data. The size of the symbols indicates the speed of the current, while the number of symbols or density of symbols suggests the amount. The largest circular symbols indicate Mediterranean outflow with rapid westward movement. Contours are σ_θ in kilograms per cubic meter

evidence of a vertical mixing process that changed the vertical stratification within the outflow layer (noted in the previous section), which will be termed a *local* mixing process. As well, the outflow entrained NACW. This latter mixing process increased the transport of the outflow and will therefore be termed a *bulk* mixing process.

a. Local mixing processes

The vertical structure of the outflow varied considerably with location (Fig. 3), but most profiles in most places could be characterized as having a two-layer structure (which we hope will not be confused with the two-layer North Atlantic/Mediterranean exchange process). As seen in density, the lower layer was a bottom mixed layer, whose thickness varied from 10% to 70% of the entire outflow layer (Fig. 3), and the upper layer was a strongly stratified interface between the bottom mixed layer and the overlying NACW. The vertical shear of the outflow current was large in both of these layers (Johnson et al., 1994a) and of opposite sign (i.e., the current increased with depth in the interface layer and decreased with depth within the bottom density mixed layer).

1) MIXING WITHIN THE INTERFACE LAYER

The interface layer was strongly stratified and also strongly sheared. Stability analysis shows that if the

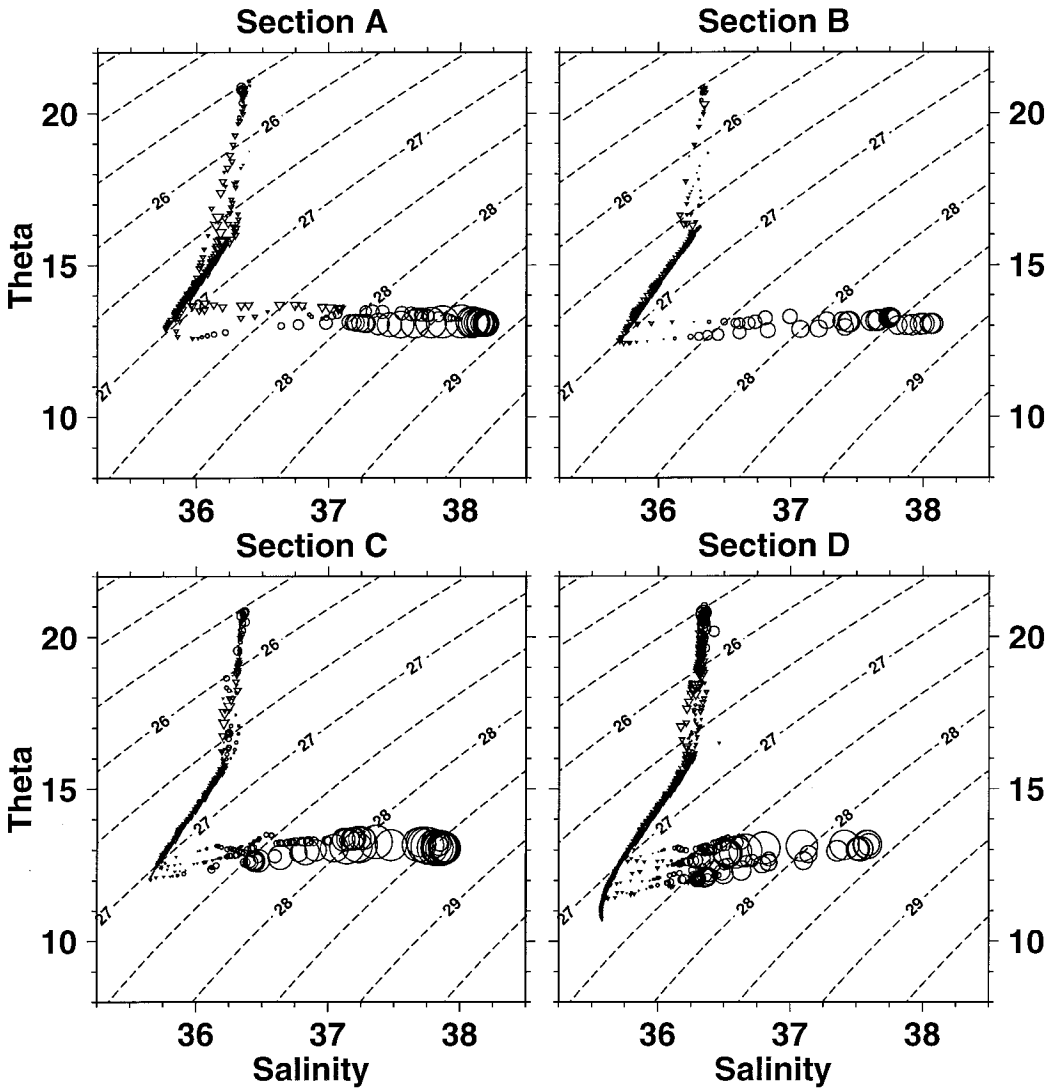

FIG. 15b. Potential temperature versus salinity as in Fig. 13a for sections E, F, G, and H. At sections G and H there were no XCPs present, and unscaled dots are used. Note that there was a substantial range in θ–S across the outflow. The warmer less salty water is toward the north. This may be seen more clearly in Fig. 14.

kinetic energy available in the sheared current is sufficient to mix the buoyancy gradient against gravity, then the current may be unstable to growing Kelvin–Helmholtz waves (Turner 1973). The usual condition for the onset of Kelvin–Helmholtz instability is that the gradient Richardson number,

$$\mathrm{Ri} = \frac{g}{\rho_o}\frac{\partial \rho}{\partial z}\Bigg/\left|\frac{\partial \mathbf{u}}{\partial z}\right|^2, \qquad (5)$$

must be less than a critical value, typically $\mathrm{Ri}_{\mathrm{crit}} \approx 0.25$, though the exact value is dependent upon the shape of the density profile as a whole (Turner 1973). In general, however, $\mathrm{Ri} \geq 0.25$ is a sufficient condition for the current to be stable. Extensive experimental research suggests that vertical mixing in stratified fluids away from the direct effects of boundaries is Richardson number dependent (Trowbridge 1992; Kunze et al. 1990; Polzin 1992; Peters et al. 1995)

To check whether shear-flow instability of this sort might be significant within the interface layer, we have estimated Ri using CTD/XCP drop pairs. A least squares fit over 20 m was used to determine the vertical gradients, $\partial\rho/\partial z$ and $\partial\mathbf{u}/\partial z$. The steric leveling method was used to bring densities to a common depth (Millard et al. 1990). The resulting Ri estimates were found to be somewhat sensitive to the length scale over which the vertical gradients were computed. For example, the 20-m interval used here gives fairly smooth Ri profiles that may overestimate the smallest values. Because of this sensitivity we are inclined to interpret only the broad pattern of the Ri profile.

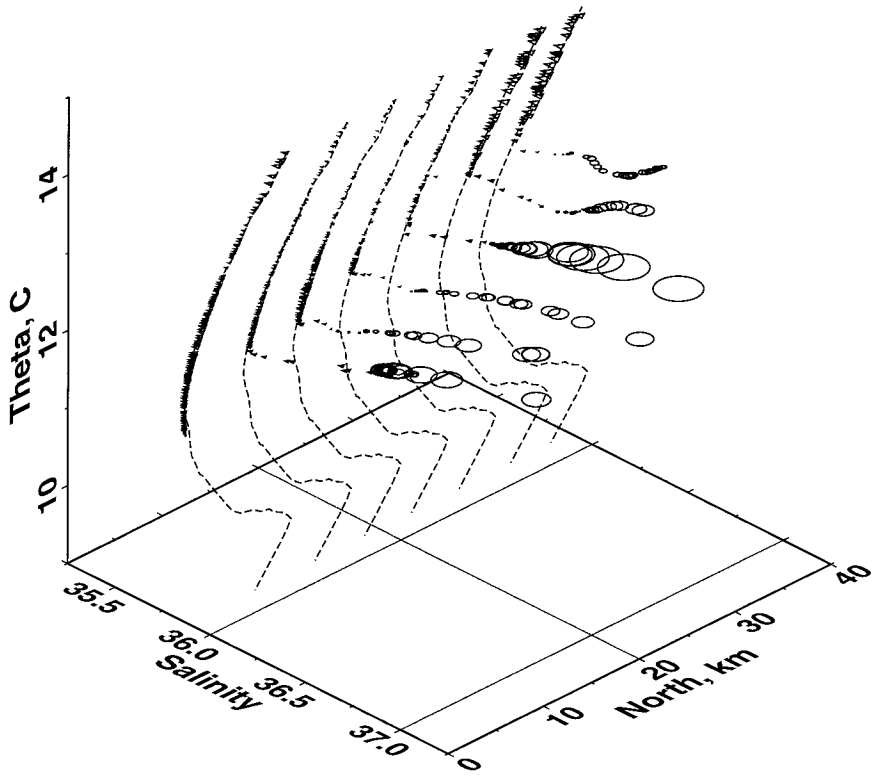

FIG. 16. Three-dimensional temperature versus salinity versus distance as in Fig. 13. Successive profiles are plotted at their northward distance from the southern end of section D. A smoothed θ–S profile from the western central Gulf of Cadiz is plotted repeatedly at each station (dashed line) to show the θ–S of NACW.

Gradient Richardson number profiles from sections A, C, and D are illustrated in Fig. 9. At section A, the outflow was found at depths below 200 m and was moving to the southwest with a maximum speed of about 0.7 m s^{-1}; Ri was less than about 1/2 within the interface from depths of about 225 to 250 m. At section C, where the outflow current was near its maximum, Ri was near 1/4 over a layer 50 m thick within the interface extending from 370 m to 420 m (Fig. 9b). These low values of Ri suggest that Kelvin–Helmholtz instability might have occurred over a thick portion of the interface layer. Here Ri had a pronounced local maximum at the depth of the velocity maximum, 430 m, since the vertical shear was very small at that depth. (The Ri was also low within the bottom density mixed layer where there was very little stratification but substantial shear as we have noted before. We do not expect that Ri is a useful measure of stability in this boundary layer.) Farther downstream, at section F, the outflow current was much reduced and Ri within the interface layer was generally considerably larger than 1/4; small values of Ri occurred in some profiles on section F, but over a much thinner layer than seen at section C, for example.

TABLE 2. Upper and lower core temperature and salinity values tabulated for each section (if the cores were readily identifiable). We follow Ambar and Howe's (1979a) definition of the upper core, the water with the maximum temperature with salinities greater than 36.3 psu. Sections L4 and L8 are located at 8°37′W and 9°2′W [not shown in Fig. 2, see Prater and Sanford (1994)].

	Lower				Upper			
Section	S (psu)	θ (°C)	σ_θ	P (dbar)	S	θ (°C)	σ_θ	P (dbar)
C	37.90	13.06	28.63	486	37.28	13.39	28.08	494
E	37.51	12.83	28.37	760	36.70	13.18	27.67	514
F	37.21	12.68	28.18	744	36.77	12.79	27.81	672
G	36.78	12.33	27.91	992	36.62	12.40	27.77	806
H	36.57	11.87	27.83	1204	36.47	12.85	27.56	758
L4	36.65	12.17	27.84	1298	36.43	12.89	27.52	744
L8	36.60	11.96	27.84	1366	36.44	12.67	27.58	764

These observations of low Ri suggest that vertical mixing driven by growing Kelvin–Helmholtz instability might have occurred within the interface layer in the high current regimes from section A through section E. There are some qualitative indications of this as well. Thorpe (1971) and Woods and Wiley (1972) have shown that Kelvin–Helmholtz instability can produce intermediate layering of the density profile. Many of the salinity or density profiles exhibited some degree of layering within the outflow above the bottom mixed layer. For instance, station 83 in section D (Fig. 9c), had two very uniform layers of salinity: a thin bottom mixed layer (only about 10 m thick in this profile) and another much thicker layer centered near 400 m, which had salinities near 36.2 psu. The entire outflow layer had *very* low gradient Richardson numbers. In section 2c, we noted similar layering at CTD station 75 (Fig. 7). There was at least one instance of an unstable density profile, suggesting the occurrence of active overturning, at CTD station 86 in section D (Fig. 9d). The density gradient near 540-m depth indicated static instability due to a layer of anomalous salinity roughly 30 m thick. More compelling evidence of vertical mixing within the interface layer was provided by Johnson et al. (1994a) who observed that the dissipation of turbulent kinetic energy was very high within the interface layer in the region from sections A to E (and see also the two examples in Fig. 7c).

2) BOTTOM MIXED LAYER

The outflow was derived from a nearly homogeneous water mass in the Mediterranean Sea, and thus the bottom density mixed layer within the Strait of Gibraltar could be ascribed to the initial condition. The bottom salinity gradually decreased along the path of the outflow (same as the core salinity) and yet a bottom density (or salinity) mixed layer remained in most profiles (Fig. 3). This indicates that the bottom mixed layer was not just a remnant of the initial condition and that there must have been active vertical mixing that stirred less saline fluid from the interface downward into the bottom mixed layer. We do not pursue the mechanisms responsible for the bottom mixing here but note that there was a source of turbulent kinetic energy at the sea floor associated with very strong bottom stress (Johnson et al. 1994a; Baringer and Price 1997). There was also a large vertical shear within the bottom mixed layer (Fig. 9), which might also have been a source of turbulent kinetic energy (Stull 1988).

Near Cape St. Vincent, much of the transport in the outflow was included within the bottom mixed layer. Thus, the mixed Mediterranean Water that finally floated off into the North Atlantic thermocline had low stratification at its core, due in part to bottom mixed layer processes. (The thickness of the entire outflow layer must also have been increased by the downstream convergence associated with the downstream reduction of the outflow current.)

b. Bulk mixing

We also attempt to characterize the flow dependence of the entrainment that caused the increase of transport described in section 4. The theory needed to guide this analysis is not nearly so well developed as is the stability analysis of stratified shear flows, but empirical evidence suggests that the layered equivalent of the Richardson number (or its inverse, the Froude number) may be relevant in some cases (Turner 1973). The Froude number for a two layer flow is

$$\mathrm{Fr}^2 = \frac{\rho_o \delta U^2}{gH\delta\rho}, \tag{6}$$

where δU is the velocity difference between layers, $\delta\rho$ is the density difference, and H is the thickness of the lowest layer. It has to be understood that the rapidly moving lower layer will entrain the relatively quiescent upper layer (this is a warning that Fr cannot be the sole parameter governing entrainment by density currents). Laboratory experiments on density currents show that when $\mathrm{Fr} \geq 1$, the moving lower layer may begin to entrain the fluid above. The entrainment rate increases very rapidly with further increases of Fr (Turner 1973; Price 1979).

To estimate a two-layer version of Fr from the continuous profiles observed in the Mediterranean outflow, we have taken the upper layer to be a layer 30 m thick just above the temperature minimum (i.e., within the eastward flowing NACW). The lower-layer properties were estimated by a vertical average over the entire outflow layer. Thus, Fr differs from Ri in the scale over which the vertical differences are taken; in this case the scale is as large as possible.

The estimated Fr were often near 1 and in some regions appear to have exceeded 1 slightly (Fig. 17). For instance, $\mathrm{Fr} = 1.2$ at station CTD 76 of section C, (Fig. 9b), echoing the instability implied by the low Ri found within the interface there. Similar values of Fr occurred also within the Strait of Gibraltar where hydraulic theory indicates that Fr could also be near 1 (Whitehead et al. 1974; Bryden et al. 1994). Smaller values, $\leq 1/2$ were found downstream at section F. The overall pattern of Fr evident in Fig. 17, and especially the occurrence of $\mathrm{Fr} \geq 1$, appears to have been roughly coincident with the regions where strong entrainment was also observed to occur, for example, near sections C and D, and on the onshore side near section E.

6. Summary and remarks

The Mediterranean outflow in the Gulf of Cadiz appears to be a nearly steady feature over decadal timescales. The height, width, path, and θ–S properties that we observed in 1988 were very similar to those de-

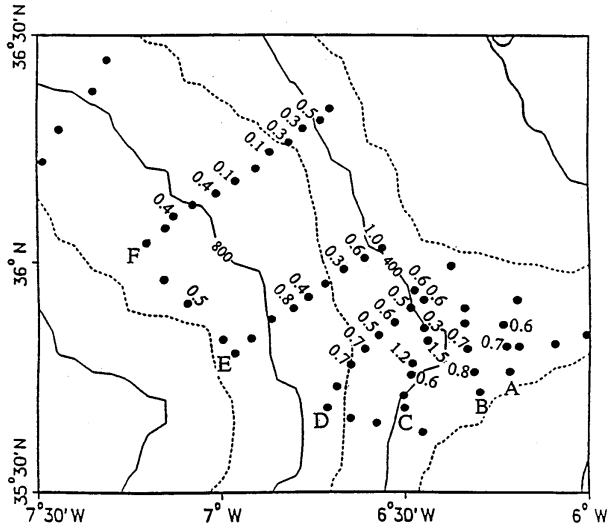

FIG. 17. Station map listing bulk Froude number estimates; Fr greater than 1 were found near section C where the most intense mixing was observed. A high Fr was also found near the northern part of section E, coincident with the impending entrainment into the upper core between section E and F.

scribed by Heezen and Johnson (1969), Madelain (1970), and Ambar and Howe (1979a). Estimates of the outflow transport have changed over this period, and the estimates reported here, approximately 0.4×10^6 m^3 s^{-1} of Mediterranean source water ($S \geq 38.4$ psu), are among the lowest yet. However, given the evident constancy of the hydrographic fields, and noting the different methods used to estimate the outflow transport, we are inclined to attribute the apparent decline in transport to changing methodology rather than a changing outflow.

a. Mixing

A primary goal of the 1988 field study was to diagnose the mixing and entrainment that reduce the salinity and density of the outflow in the Gulf of Cadiz. One simple and traditional diagnostic variable is the alongstream profile of maximum salinity. Our observations of maximum salinity are within 0.05 of those described by Heezen and Johnson (1969) and indicate a rather gradual decrease of outflow salinity, which in turn implies a quasi-uniform mixing process (Fig. 12). However, the maximum salinity may not make a good measure of the average properties of an outflow 100 m thick; for example, the maximum salinity was usually found very close to the bottom, and well below the maximum currents. A more representative salinity can now be formed as the velocity-weighted average salinity across a section. This shows a much more rapid decrease of outflow salinity (decreasing by 1.1 between sections A and D, while the maximum salinity decreases by less, 0.6) and shows that the strongest entrainment occurred where the outflow began to descend the continental slope.

The outflow became neutrally buoyant near Cape St. Vincent where the maximum salinity was about 36.6 psu. The velocity-weighted salinity had already decreased to a similar value by section D, and thus the final middepth separation of the Mediterranean Water was decided along the first 80 km of its path through the Gulf of Cadiz. So far as the mixing process goes, this rapid decrease of the outflow salinity anomaly is the most important observation from this field study.

The transport of the outflow increased coincident with this decrease in salinity. Thus, the mixing is, in large part, an entrainment process in which fresher NACW was incorporated into the descending outflow. The outflow transport increased from about 0.7×10^6 m^3 s^{-1} at section A at the west end of the Strait of Gibraltar (where the outflow was already partially mixed Mediterranean Water) to about 1.5×10^6 m^3 s^{-1} 85 km farther downstream at section F, where the outflow was then made up of one part pure Mediterranean source water to about three parts NACW. Because Mediterranean source water is only a small fraction of the mixed Mediterranean Water that enters the North Atlantic, it will be difficult to detect the impact on North Atlantic hydrography of the observed man-induced, Mediterranean Sea salinity increase (Rohling and Bryden 1992). (Indeed, given the recipe for the mixed water, it would appear that any change in the middepth Mediterranean Water in the North Atlantic would be more likely caused by changes in NACW rather than the Mediterranean source component.)

The processes that caused the mixing can be inferred from the structure of the outflow. In the region around section C where mixing was most intense, the currents were also the largest observed, in excess of 1 m s^{-1}. There was a very thick, and strongly sheared, interface between the lower portion of the outflow and the eastward flowing NACW above. Within this interface layer the gradient Richardson numbers were near critical, suggesting that the interface was unstable to Kelvin–Helmholtz waves. There was intense dissipation within this layer as well, confirming that there was active turbulent mixing (Johnson et al. 1994b). The bulk Froude number was slightly supercritical, Fr $\geq$ 1, near the Strait of Gibraltar coincident with the vigorous entrainment inferred from the salinity and transport calculations (Figs. 9, 12, and 17). Farther from the strait, at section F, where entrainment and mixing were greatly reduced, the bulk Froude numbers were typically well below 1 (subcritical). This spatial coincidence of low gradient Richardson numbers (and large bulk Froude numbers) with strongest mixing and entrainment suggests that the turbulent energy source required for vertical mixing was the kinetic energy of the mean flow. In turn, the mean kinetic energy was produced mainly by the release of potential energy as the dense outflow descended the continental slope (Baringer and Price 1997), and thus

the observed correspondence between strong mixing and flow down steep slopes seems almost inevitable.

The Mediterranean outflow is derived from a nearly homogeneous source, the Mediterranean Intermediate Waters, and so began in the eastern Strait of Gibraltar with very low stratification. Vertical mixing at the interface produced high stratification within the westward flowing layer around sections A though E, though a bottom density mixed layer was also evident in most profiles (Fig. 3). Farther downstream near Cape St. Vincent the interface layer was a smaller fraction of the total outflow and the bottom mixed layer was often quite thick. We speculate that the bottom mixed layer thickness increased downstream of section E on account of both turbulent erosion driven by the bottom stress and by the alongstream convergence that must have accompanied the reduction of the outflow speed. The mixed Mediterranean Water at Cape St. Vincent thus had low stratification at its core, though not directly as a consequence of its origin.

b. Spreading and descent

The width of the Mediterranean outflow increased from about 10 km while still confined within the Strait of Gibraltar, to a maximum of about 80 km by about 200 km downstream. Over the same distance the center of mass descended from 400 m to about 800 m. The outflow was sufficiently wide that the onshore and offshore sides necessarily descended the continental slope at very different rates; the shallow onshore side descended only about 200 m, while the deeper offshore side descended about 1000 m (Fig. 8). Thus, the spreading and the descent of the outflow are closely linked. From an analysis of the overall energy budget of the outflow (Baringer and Price 1997), it is evident that bottom and interfacial stress were essential in causing the outflow to descend topography (geostrophic adjustment alone was not enough) and by extension were also the processes that caused or allowed the outflow to spread out.

Some depth-dependent frictional effects are evident in the Ekman-like veering with height observed above the velocity maximum (Fig. 9). On average, this veering was about 8° (Fig. 10), which can account for only about 10%–20% of the observed spreading. Most of the spreading was due to an across-stream divergence; the current on the onshore side remained nearly parallel to isobaths, while the current on the offshore side descended across isobaths rather steeply.

This spreading and asymmetric descent combined with mixing caused the outflow to develop cross-stream differences in θ–S properties along isopycnals. The source water had a very narrow range of θ–S. As the outflow descended and spread out over the continental slope, the onshore side of the outflow remained higher in the water column and, thus, mixed with warmer North Atlantic Central water than did the deeper offshore side (Fig. 14). By about 100 km downstream, the cross-stream θ variation on an isopycnal was a little more than 2°C, with the warmer water found on the onshore side of the outflow.

Near Cape St. Vincent, the outflow had developed two fairly distinct modes or cores whose θ–S properties were acquired as described above. The shallower core had (θ, S) = (12.89°C, 36.43 psu) and settled into the thermocline at about 750 m, while the lower core had (θ, S) = (12.17°C, 36.65 psu) and settled out at around 1300 m. The occurrence of two cores (rather than a smoothly varying transport as a function of density class) appears to be a consequence of topographic steering, which split the outflow into two partially connected branches not long after the outflow began to descend into the Gulf of Cadiz. Bottom mixed layer processes produced vertically homogeneous water as the final product of the outflow.

Acknowledgments. This research was sponsored by the U.S. Office of Naval Research through Grants N00014-89-J-1053 and N00014-90-J-1474 and by a Secretary of the Navy Fellowship to M.O.B. We are grateful to the scientific party of the 1988 Gulf of Cadiz Expedition and the crew of the R/V *Oceanus* for their invaluable assistance during the field work. Special thanks go to Thomas Sanford who made this project possible. Thanks also to John Dunlap and Robert Dever for providing engineering support, to Eric Kunze who developed the XCP acquisition software, to Maureen Kennelly who performed much of the data processing, and to M. Dickson Allison and Mark Prater who assisted with the data analysis. The authors would also like to thank Rolf Lueck, Harry Bryden, Mike McCartney, Larry Pratt, and Paola Rizzoli for their thoughtful comments throughout the course of this research and to Eric Kunze and the anonymous referees whose comments helped improve this manuscript.

REFERENCES

Ambar, I., 1983: A shallow core of Mediterranean water off western Portugal. *Deep-Sea Res.,* **30,** 677–680.

——, and M. R. Howe, 1979a: Observations of the Mediterranean outflow. I. Mixing in the Mediterranean outflow. *Deep-Sea Res.,* **26** (A), 535–554.

——, and ——, 1979b: Observations of the Mediterranean outflow. II. The deep circulation in the vicinity of the Gulf of Cadiz. *Deep-Sea Res.,* **26** (A), 555–568.

Armi, L., and W. Zenk, 1984: Large lenses of highly saline Mediterranean Water. *J. Phys. Oceanogr.,* **14,** 1560–1576.

——, and D. M. Farmer, 1988: The flow of Mediterranean water through the Strait of Gibraltar. *Progress in Oceanography,* Vol. 21, Pergamon Press, 1–106.

Baringer, M. O., 1993: Mixing and dynamics of the Mediterranean outflow. Ph.D. thesis, Massachusetts Institute of Technology/Woods Hole Oceanographic Institution Joint Program in Oceanography, Cambridge, MA, WHOI-93-52, 244 pp. [Available from Woods Hole Oceanographic Institute, Woods Hole, MA 02543.]

——, and J. F. Price, 1997: Momentum and energy balance of the Mediterranean outflow. *J. Phys. Oceanogr.*, **27,** 1678–1692.

Bethoux, J. P., 1979: Budgets of the Mediterranean Sea. Their dependence on local climate and on the characteristics of the Atlantic waters. *Oceanol. Acta,* **2,** 157–163.

Bryden, H. L., E. C. Brady, and R. D. Pillsbury, 1989: Flow through the Strait of Gibraltar. *Seminario Sobre la Oceanografia Fisica del Estrecho de Gibraltar, Madrid 24–28 Octubre 1988,* J. L. Almazan, H. Bryden, T. Kinder, and G. Parrilla, Eds., Sociedad Espanola de Estudios para la Communicacion Fija a Traves del Estrecho de Gibraltar, 166–194.

——, J. C. Candela, and T. H. Kinder, 1994: Exchange through the Strait of Gibraltar. *Progress in Oceanography,* Vol. 33, Pergamon Press, 201–248.

Candela, J. C., 1991: The Gibraltar Strait and its role in the dynamics of the Mediterranean Sea. *Dyn. Atmos. Oceans,* **15,** 267–299.

——, C. D. Winant, and H. L. Bryden, 1989: Meteorologically forced subinertial flows through the Strait of Gibraltar. *J. Geophys. Res.*, **94,** 12 667–12 679.

——, ——, and A. Ruiz, 1990: Tides in the Strait of Gibraltar. *J. Geophys. Res.,* **95,** (C5), 7313–7335.

Defant, A., 1961: *Physical Oceanography.* Vol. I. Pergamon Press, 729 pp.

Ezer, T., and G. L. Weatherly, 1991: Small-scale spatial structure and long-term variability of near-bottom layers in the HEBBLE area. *Mar. Geol.,* **99** (3/4), 319–328.

Heezen, B. C., and G. L. Johnson, 1969: Mediterranean under-current and microphysiography west of Gibraltar. *Bull. Inst. Oceanogr., Monaco,* **67** (1382), 1–97.

Hinrichsen, H. H., M. Rhein, R. H. Käse, and W. Zenk, 1993: The Mediterranean water tongue and its chlorofluoromethane signal in the Iberian Basin in early summer 1989. *J. Geophys. Res.*, **98,** 8405–8412.

Hopkins, T. S., 1978: Physical processes in the Mediterranean basins. *Estuarine Transport Processes,* B. Kjerve, Ed. University of South Carolina Press, 269–310.

Howe, M. R., M. I. Abdullah, and S. Deetae, 1974: An interpretation of the double *T–S* maxima in the Mediterranean using chemical tracers. *J. Mar. Res.,* **32,** 377–386.

Johnson, G. C., and T. B. Sanford, 1992: Secondary circulation in the Faroe Bank Channel outflow. *J. Phys. Oceanogr.,* **22,** 927–933.

——, ——, and M. O. Baringer, 1994a: Stress on the Mediterranean outflow plume. Part I: Velocity and water property measurements. *J. Phys. Oceanogr.,* **24,** 2072–2083.

——, R. G. Lueck, and T. B. Sanford, 1994b: Stress on the Mediterranean outflow plume. Part II: Turbulent dissipation and shear measurements. *J. Phys. Oceanogr.,* **24,** 2084–2092.

Kennelly, M. A., J. H. Dunlap, T. B. Sanford, E. L. Kunze, M. D. Prater, and R. G. Drever, 1989a: The Gulf of Cadiz Expedition: R/V *Oceanus* Cruise 202. Tech. Rep. APL-UW TR 8914, 115 pp. [Available from Applied Physics Laboratory, University of Washington, Seattle, WA 98105.]

——, M. D. Prater, J. H. Dunlap, E. L. Kunze, and T. B. Sanford, 1989b: XCP data from the Gulf of Cadiz Expedition: R/V *Oceanus* Cruise 202. Tech. Rep. APL-UW TR 8925, 206 pp. [Available from Applied Physics Laboratory, University of Washington, Seattle, WA 98105.]

——, T. B. Sanford, and T. W. Lehman, 1989c: CTD data from the Gulf of Cadiz Expedition: R/V *Oceanus* Cruise 202. Tech. Rep. APL-UW TR 8917, 129 pp. [Available from Applied Physics Laboratory, University of Washington, Seattle, WA 98105.]

Kenyon, N. H., and R. H. Belderson, 1973: Bed forms of the Mediterranean undercurrent observed with side-scan sonar. *Sediment. Geol.,* **9,** 77–99.

Kinder, T. H., and H. L. Bryden, 1987: The 1985–1986 Gibraltar Experiment: Data collection and preliminary results. *Eos, Trans. Amer. Geophys. Union,* **68,** 786–787, 793–795.

Kunze, E., A. J. Williams III, and M. G. Briscoe, 1990: Observations of shear and vertical stability from a neutrally buoyant float. *J. Geophys. Res.*, **95** (C10), 18 127–18 142.

Lacombe, H., and P. Tchernia, 1960: Quelques traits generaux de l'hydrologie Mediterranee. *Cah. Oceanogr.,* **12,** 527–547.

——, and C. Richez, 1982: The regime of the Strait of Gibraltar. *Hydrodynamics of Semi-Enclosed Seas,* J. C. J. Nihoul, Ed., Elsevier Oceanography Series, Vol. 34, Elsevier, 13–73.

——, J. C. Gascard, J. Gonella, and J. P. Bethoux, 1981: Response of the Mediterranean to the water and energy fluxes across its surface, on seasonal and interannual scales. *Oceanol. Acta,* **14,** 247–255.

Lynch, J., and R. Lueck, 1989: Expendable Dissipation Profiler (XDP) data from the Mediterranean Out-flow Experiment R/V *Oceanus* Cruise 202 leg V. Tech. Rep. JHU-CBI TR89-01, 284 pp.

Macdonald, A. M., J. Candela, and H. L. Bryden, 1993: Heat transport in the Strait of Gibraltar. *The Seasonal and Interannual Variability of the Western Mediterranean Sea,* P. E. La Violette, Ed., Elsevier, 13–32.

Madelain, F., 1970: Influence de la topographie du fond sur l'ecoulment Mediterraneen entre le Detroit de Gibraltar et le Cap Saint-Vincent (Influence of topography on the Mediterranean outflow between the Strait of Gibraltar and Cape St. Vincent). *Cah. Oceanogr.,* **22,** 43–61.

Millard, R. C., W. B. Owens, and N. P. Fofonoff, 1990: On the calculation of the Brunt–Väisälä frequency. *Deep-Sea Res.,* **37,** 167–181.

Nielsen, J. N., 1912: Hydrography of the Mediterranean and adjacent waters. Report of the Danish oceanographic expedition 1908–1910 to the Mediterranean and adjacent waters. Tech. Rep. 1, Copenhagen, 72–191.

Ochoa, J., and N. A. Bray, 1991: Water mass exchange in the Gulf of Cadiz. *Deep-Sea Res.,* **38** (S1), 5465–5503.

Perkin, R. G., and E. L. Lewis, 1980: The practical salinity scale 1978: Fitting the data. *IEEE J. Oceanic Eng.,* **OE-5,** 9–16.

Peters, H., M. C. Gregg, and T. B. Sanford, 1995: Detail and scaling of turbulent overturns in the Pacific equatorial undercurrent. *J. Geophys. Res.*, **100** (C9), 18 349–18 368.

Polzin, K. L., 1992: *Observations of Turbulence, Internal Waves and Background Flows: An Inquiry into the Relationships Between Scales of Motion.* Ph.D. dissertation, Massachusetts Institute of Technology/Woods Hole Oceanographic Institution Joint Program in Oceanography, WHOI-92-39. [Available from Woods Hole Oceanographic Institute, Woods Hole, MA 02543.]

Prater, M. D., 1991: A method for depth and temperature correction of expendable probes *J. Atmos. Oceanic Technol.,* **8,** 888–894.

——, and T. B. Sanford, 1994: A meddy off Cape St. Vincent. Part I: Description. *J. Phys. Oceanogr.,* **24,** 1572–1586.

Price, J. F., 1979: On the scaling of stress-driven entrainment experiments. *J. Fluid Mech.,* **90,** 509–529.

——, M. O. Baringer, R. G. Lueck, G. C. Johnson, I. Ambar, G. Parrilla, A. Cantos, M. A. Kennelly, and T. B. Sanford, 1993: Mediterranean outflow mixing and dynamics. *Science,* **259,** 1277–1282.

Reid, J. L., 1979: On the contribution of the Mediterranean Sea outflow to the Norwegian–Greenland Sea. *Deep-Sea Res.,* **26,** 1199–1223.

Rhein, M., and H. H. Hinrichsen, 1993: Modification of Mediterranean Water in the Gulf of Cadiz, studied with hydrographic, nutrient and chlorofluoromethane data. *Deep-Sea Res.,* **40,** 267–291.

Rohling, E. J., and H. L. Bryden, 1992: Man-induced salinity and temperature increases in Western Mediterranean Deep Water. *J. Geophys. Res.*, **97** (C7), 11 191–11 198.

Sanford, T. B., 1971: Motionally induced electric and magnetic fields in the sea. *J. Geophys. Res.,* **76,** 3476–3492.

——, R. G. Drever, and J. H. Dunlap, 1978: A velocity profiler based on the principles of geomagnetic induction. *Deep-Sea Res.,* **25,** 183–210.

——, E. A. D'Asaro, E. Kunze, J. H. Dunlap, R. G. Dever, M. A. Kennelly, M. D. Prater, and M. S. Horgan, 1993: An XCP user's

guide and reference manual. Tech. Rep. APL-UW TR 9309, 59 pp. [Available from Applied Physics Laboratory, University of Washington, Seattle, WA 98105.]

Seidler, G., 1968: Haufigkeitsverteil von Wasserarten im Ausstrombereich von Meeresstrassen. *Kiel. Meeresforch.,* **24** (2), 59–65.

Smith, P. C., 1975: A streamtube model for bottom boundary currents in the ocean. *Deep-Sea Res.,* **22,** 853–873.

Stanton, B. R., 1983: Low frequency variability in the Mediterranean outflow west of Gibraltar. *Deep-Sea Res.,* **30** (7A), 743–761.

Stommel, H., H. Bryden, and P. Mangelsdorf, 1973: Does the Mediterranean outflow come from great depth? *Pure Appl. Geophys.,* **105,** 879–889.

Stull, R. B., 1988: *An Introduction to Boundary Layer Meteorology.* Kluwer Academic, 666 pp.

Sverdrup, H. U., M. W. Johnson, and R. H. Fleming, 1942: *The Oceans, Their Physics, Chemistry and General Biology.* Prentice-Hall, 1087 pp.

Thorpe, S. A., 1971: Experiments in the instability of stratified shear flows: Miscible fluids. *J. Fluid Mech.,* **46,** 299–319.

——, 1976: Variability of the Mediterranean undercurrent in the Gulf of Cadiz. *Deep-Sea Res.,* **23,** 711–724.

Trowbridge, J. H., 1992: A simple description of the deepening and structure of a stably stratified flow driven by a surface stress. *J. Geophys. Res.,* **97** (C10), 15 529–15 543.

Turner, J. S., 1973: *Buoyancy Effects in Fluids.* Cambridge University Press, 368 pp.

Whitehead, J. A., A. Leetma, and R. A. Knox, 1974: Rotating hydraulics of strait and sill flows. *Geophys. Fluid Dyn.,* **6,** 101–125.

Woods, J. D., and R. L. Wiley, 1972: Billow turbulence and ocean microstructure. *Deep-Sea Res.,* **19,** 87–121.

Worthington, L. V., and W. R. Wright, 1970: *North Atlantic Ocean Atlas of Potential Temperature and Salinity in the Deep Water Including Temperature, Salinity and Oxygen Profiles from the Erika Dan Cruise of 1962.* Woods Hole Oceanographic Institution Atlas Series, Woods Hole Oceanographic Institution, 24 pp. and 58 plates.

Wust, G., 1935: *The Stratosphere of the Atlantic Ocean* (translated in 1978 by W. J. Emery from Schichtung und Zirkulation des Atlantischen Ozeans, Die Stratosphare in *Wissenschaftliche Ergebnisse der Deutschen Atlantischen Expedition Auf-dem Forschungs-Und Vermessungsschiff ''Meteor'', 1925–1927,* **6,** 1–2, 180 pp.). Amerind, 112 pp.

Zenk, W., 1970: On the temperature and salinity structure of the Mediterranean water in the N. E. Atlantic. *Deep-Sea Res.,* **17,** 627–632.

——, 1975a: On the Mediterranean outflow west of Gibraltar. *''Meteor'' Forsch.-Ergebn.,* **16** (A), 23–34.

——, 1975b: On the origin of the intermediate double-maxima in *T*/*S* profiles from the North Atlantic. *''Meteor'' Forsch.-Ergebn.,* **16** (A), 35–43.